Electronic decay processes of photoexcited 2p resonances of atomic Ar, K, and Ca

M. Meyer,* E. von Raven, and B. Sonntag
II. Institut für Experimentalphysik, Universität Hamburg, Luruper Chaussee 149, D-22761 Hamburg, Federal Republic of Germany

J. E. Hansen
Van der Waals-Zeeman Laboratory, University of Amsterdam, Valckenierstraat 65, NL-1018 XE Amsterdam, The Netherlands
(Received 24 August 1993; revised manuscript received 20 December 1993)

An experimental and theoretical study is presented of the $2p \rightarrow ms,nd$ inner-shell excitations in the elements Ar, K, and Ca with special emphasis on the $2p \rightarrow 3d$ excitations. The present work is mainly concerned with investigations of K and Ca. An interpretation is given of the resonant Auger spectra in which it is shown that the difference in collapse of the 3d wave function in the presence of holes in the 2p shell compared to holes in the 3p shell leads to qualitative differences between the three atoms. In Ar, shake effects are very strong between the initial state with one 2p hole and the final state with two holes in the 3p shell due to the fact that the 3d orbital collapses between the two. However, in K and Ca the 3d orbital is collapsed in both states and shake effects are found to be much smaller for this excitation. In contrast, for K and Ca it is predicted that the 4d orbital will show strong shake effects. The collapse of the 3d orbital in the final state of all three atoms leads to resonant Auger spectra which are very different from those following direct ionization in the 2p shell. The details of the resonant Auger spectra depend on the degree of collapse; we discuss the differences in the observed spectra in terms of the relative strengths of the electrostatic $3p \leftrightarrow 3p$ and $3p \leftrightarrow 3d$ interactions in the three elements. The second-step Auger decays in K and Ca are studied both experimentally and theoretically.

PACS number(s): 32.80.Hd, 32.80.Fb, 32.80.Dz, 31.20.Tz

I. INTRODUCTION

Inner-shell resonances of atoms are strongly influenced by electron correlation. The investigation of these resonances by photoelectron spectroscopy therefore provides detailed information about the character and the strength of the many-electron interactions and about the dynamics of the decay processes. Especially the strong $3p \rightarrow 3d$ and $4d \rightarrow 4f$ resonances in the 3d transition elements and the lanthanides, respectively, have attracted a large amount of interest during the past years [1–4 and references therein]. However, the investigation of deep inner-shell resonances, which are defined in this article as resonances with excitation energies $E_{res} > 200$ eV, e.g., $2p \rightarrow 3d$ for the 3d transition elements and $3d \rightarrow 4f$ for the rare earth elements, offers some special advantages. The interaction between the deep core hole and the outer excited electron is strongly reduced, which, for example, results in relatively simple excitation spectra. On the other hand, a hole in a deep subshell allows a variety of decay processes to occur, resulting in a large number of different lines in the electron spectrum (cf. Fig. 1), which reflect the different interactions in the initial excited state as well as in the final ionic state. Due to the small oscillator strengths of the deep inner-shell resonances in comparison with the outer-shell resonances and due to the small number of suitable light sources for the relevant region of photon energy, 200 eV $< \hbar\omega <$ 1000 eV, the knowledge of the $2p \rightarrow nd$ resonances in the 3d transition elements and the $3d \rightarrow nf$ resonances in the rare earth elements is very limited. It is mainly based on absorption and ion-yield spectra of some particular elements (Ar [5,6]; K [7–9]; Ca [8–10]; Mn [11]; Xe, Cs, and Ba [12]; and Sm and Tm [13]), which show discrete resonances just below the main 2p (Ar, K, Ca, and Mn) and 3d thresholds (Xe, Cs, Ba, Sm, and Tm). More detailed studies of the decay channels of these resonances have been performed only on the rare gas Ar [14–18] and on a few other atoms (Ca [19] and Eu [20]). In this paper we present an extensive and detailed investigation, by electron spectroscopy and Hartree-Fock (HF) calculations, as well as configuration interaction (CI) calculations, of the $2p \rightarrow ms,nd$ resonances of atomic Ar, K, and Ca with special emphasis on the $2p \rightarrow 3d$ excitations. The special position of these atoms in the Periodic Table with respect to the 3d transition elements and the resulting sensitivity of the 3d wave function to its actual environment in these atoms form the physical background for the present study.

As an introduction, a typical electron spectrum emitted following the decay of a 2p core resonance, a so-called resonant Auger spectrum, is displayed in Fig. 1. It was recorded by exciting the K* $2p^5(^2P_{3/2})3s^23p^63d4s$ resonance (neither the full 1s and 2s shells nor, in the case of the 2p hole states, the full 3s and 3p shells are shown explicitly in the following) with photons of 297.0 eV energy. Prominent line structures, which represent different decay processes, are observed in two different kinetic-energy regions. Direct ionization of the outer shells and/or autoionization into K^+ continua cause the lines in the region 190 eV $< E_{kin} <$ 280 eV. The main 3p and 3s

*Present address: LURE, Bâtiment 209D, Université Paris-Sud, F-91405 Orsay Cedex, France.

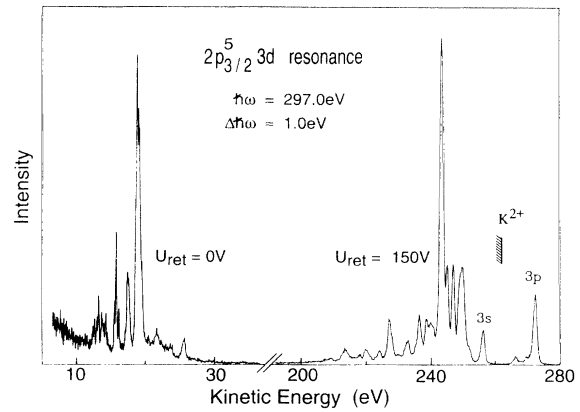

FIG. 1. Electron spectrum of atomic K photoexcited at the K* $2p^5(^2P_{3/2})3s^23p^63d4s$ resonance ($\hbar\omega=297.0$ eV). The high- and low-kinetic-energy parts are given on different energy scales; the intensities of both parts are not adjusted to each other. [Monochromator bandwidth $\Delta\hbar\omega=1.0$ eV; resolution of the electron analyzer $\Delta E_{\rm kin}=0.01(E_{\rm kin}-eU_{\rm ret})$.]

photolines at $E_{\rm kin}=272.3$ and 256.0 eV, respectively, enhanced by the decay K* $2p^53d4s\rightarrow K^+$ $2p^63s^23p^5(3d$ or $4s)+\epsilon l$ and K^+ $2p^63s^13p^6(3d$ or $4s)+\epsilon l$, respectively, are indicated. The four levels of the K^+ $3p^54s$ configuration and the two levels of the K^+ $3p^53d$ ^3P term found in a high-resolution spectrum by Süzer *et al.* [21] cannot be resolved in the present work mainly due to the monochromator bandpass ($\Delta\hbar\omega\simeq1.0$ eV) used. Besides these photolines very complex and much more intense line structures arise in the range 210 eV $\le E_{\rm kin}\le$ 255 eV. They are due to Auger-like decays of the resonantly excited $2p$ hole state to states of the singly charged ion, such as K^+ $3s^03p^63d4s$, $3s^13p^53d4s$, and $3s^23p^43d4s$. The binding energies of the individual states can be determined from $E_B=\hbar\omega-E_{\rm kin}$. The strongest lines (240 eV $< E_{\rm kin}<$ 255 eV), which are assigned to the decay K* $2p^53d4s\rightarrow K^+$ $2p^63s^23p^43d4s+\epsilon l$ involving the creation of two $3p$ holes in the final state, are the most characteristic features of the electron spectra emitted upon the decay of the $2p\rightarrow3d$ resonances in Ar, K, and Ca. Energy splitting and intensity distribution of the K^+ $3p^43d4s$ multiplet are mainly determined by the strength of the $3p\leftrightarrow3d$ and $3p\leftrightarrow3p$ interactions (the interaction with the $4s$ electron is much weaker) and therefore both are very sensitive to the degree of collapse of the $3d$ wave function in the ionic state.

In the region of low kinetic energies 5 eV $< E_{\rm kin}<$ 35 eV (left-hand side of Fig. 1), another group of resonantly enhanced lines is observed. The origin of these lines is the subsequent decay of those K^+ states that are populated by autoionization of the $2p$ resonances *and* lie above the lowest K^{2+} threshold. The investigation of these Auger lines, mainly K^+ $3p^43d4s\rightarrow K^{2+}$ $3p^5+\epsilon l$, yields complementary information about the K^+ states. Except for the fluorescence decay and possible decay processes, which result in free electrons with low kinetic energies ($E_{\rm kin}<5$ eV), the recorded spectra comprise all possible decay processes of the $2p$ resonances. As a result, the cross sections for the production of singly and doubly charged ions, which were obtained from the ion-yield spectra for all three atoms Ar [6], K, and Ca [8,9], can be partitioned into cross sections for the production of individual ionic states and the differences in the transition probabilities reflect the different interaction strengths.

In this work, the results obtained from such electron spectra taken in the excitation region of the $2p$ resonances as well as the $2p$ thresholds for the three atoms are compared with the results of calculations. In Secs. II and III we briefly describe our experimental setup and the method of calculation, respectively. The results for the individual elements are summarized in Secs. IV A–IV C and, finally, systematic trends characterizing the sequence Ar-K-Ca are presented in Sec. V.

II. EXPERIMENT

The experimental investigations were performed at the FLIPPER I wiggler/undulator beamline at the Hamburger Synchrotronstrahlungslabor HASYLAB [22]. The Ca and K atomic beams were produced by an oven indirectly heated by electron bombardment and collimated by a separately heated nozzle. In the case of Ar, argon gas of high purity (99.99%) was led to the reaction volume through a thin capillary (diameter about 1 mm). The atomic beam crosses the monochromatized synchrotron radiation in the acceptance volume of a cylindrical mirror analyzer (CMA). The CMA collects only electrons which are emitted close to the magic angle (54°44′) with respect to the main axis of the polarization ellipse of the light. For the measurements on the metallic vapors K and Ca, a CMA covering an azimuth angle of 180° was used, i.e., the lower half of the CMA is cut off to provide adequate space for the atomic beam source. For Ar we used a CMA with full azimuth of 360° to achieve a very high acceptance (1.6% of 4π). For these geometries it can be shown (see, e.g., [23]) that the intensities in the electron spectra are independent of angular distribution effects of the photoelectrons and it is possible to determine relative partial cross sections directly. The resolution of both analyzers is $\Delta E_{\rm kin}/E_{\rm kin}=0.8\%$. To improve this value for the analysis of the high-kinetic-energy region of the spectra, it is possible to retard the fast electrons by a constant electric field before they enter the CMA. The retardation optics consists of two semihemispherical shells of different radii, which are installed isolated from each other and centered on the source volume, in the entrance area of the CMA. Small slits at the positions of the electron trajectories allow the electrons to reach the entrance slit of the CMA. Applying a negative voltage $-U_{\rm ret}$ between both shells, a total resolution $\Delta E_{\rm kin}=0.01(E_{\rm kin}-eU_{\rm ret})$ could be achieved. Due to the extended reaction volume some electrons having a nonradial velocity component with respect to the central symmetric retardation field are deflected [24] and the virtual source volume exceeds the acceptance volume of the CMA for high values of $U_{\rm ret}$. Therefore the transmission of the analyzer decreases strongly at high values of $U_{\rm ret}$ and this limits in practice the attainable resolving power of the analyzer. The transmission as a function of the ratio $E_{\rm kin}/eU_{\rm ret}$ was determined separately, by measuring a

series of Ar $L_{23}M_{23}M_{23}$ Auger spectra with different U_{ret}, and taken into account for the evaluation of the electron spectra. The bandwidth of the monochromator was about 0.6 eV at a photon energy of $\hbar\omega=240$ eV for the Ar spectra and about 1.0 and 1.8 eV at $\hbar\omega=300$ and 350 eV close to the 2p excitation energies of atomic K and Ca, respectively.

III. CALCULATIONS

In a single-configuration model it could be expected that the outer Rydberg electron would not participate in the subsequent Auger decay but act as a spectator to the decay of the 2p hole with the result that to first order the Auger spectrum would look like the normal Auger spectrum connected with the decay of the 2p hole. This so-called "spectator model" [14,25] is useful in many cases but does not apply in the case of the resonant $2p\rightarrow 3d$ Auger spectra in Ar [16] and in Ca [19] because of the strength of, in particular, the $3p\leftrightarrow 3d$ interaction in the final state. On the other hand, this interaction leads mainly to a redistribution of decay strength within each final configuration and only to a lesser degree to a redistribution between configurations. This has consequences, for example, for the probabilities for a second-step Auger decay for which the spectator model works quite well as discussed later.

However, due to the breakdown of the spectator model for the resonant Auger spectra, detailed calculations are necessary which must determine the different interaction strengths rather precisely. Here we have used the suite of programs written by Cowan [26] which can be used to perform CI calculations with HF basis states. We note that the programs automatically apply a correlation correction to the average energy of each configuration. This correction is based on a free-electron-gas approximation [26]. In practice only a limited number of configurations can be included in such calculations and to obtain reasonable agreement with the observed energy levels with this approach it is, in addition, usually necessary to scale down the theoretical interaction parameters for a particular configuration with an empirical factor. The justification for this practice is that it has been found (rigorously for the first time by Rajnak and Wybourne [27]) that the effect of high-lying weakly interacting configurations on a low-lying configuration is to reduce the values of the Slater integrals for the low-lying configuration mirroring the squeezing of the lower configuration because the higher levels are more perturbed than the lower ones. The effect of scaling is particularly important in the present case. This is because the structure of the $3p^4 3d$ configuration is strongly dependent on the ratio between the strength of the $3p\leftrightarrow 3p$ and the $3p\leftrightarrow 3d$ interaction as first noticed by Cowan [28]. The $3p\leftrightarrow 3p$ interaction gives rise to the separation between the three $3p^4$ parent terms ^3P, ^1D, and ^1S and if the $3p\leftrightarrow 3d$ interaction is weak, as it is before the 3d collapse, the $3p^4 3d$ levels are clustered around the positions of the three parent terms. The collapse of the 3d orbital increases the $3p\leftrightarrow 3d$ interaction and causes a large mixing of the $3p^4$ parent terms for certain LS symmetries. Since the Auger decay probabilities depend on the parent term, it is clear that it is necessary to have a good determination of the mixing, i.e., the relative strength of the $F^2(3p,3p)$ and the $G^1(3p,3d)$ integrals in order to be able to predict the details of the Auger spectrum.

A. Choice of scaling factors

We note that in our previous study of Ca [19] we did not use scaling, but instead very large scale calculations which would be very difficult to extend to K because of the presence of the unpaired 4s electron. Thus we have chosen for the computationally simpler approach of using scaling for K. Since the final levels in K II are unknown and the analysis of K III [29] is deficient, as discussed below, we resorted to determine the K scaling factors by interpolating between Ar II and Ca IV.

We have determined scaling factors of 85% for $F^2(3p,3p)$ and 80% for the $G^k(3p,3d)$ integrals for Ca from the known $3s^2 3p^4 3d$ structure [30] in Ca IV. In both Ar II and Ca IV, a scaling factor of 85% for the configuration interaction integrals places the $3s3p^6$ term in the right position relative to the ground state while the $3p^4(^1D)3d\ ^2S$ term is located too high, reflecting the need to include the whole $3p^4(^1D)nd/\epsilon d\ ^2S$ series in order to describe the interaction correctly [31]. The result is a too large 3d component in the $3s3p^6$ term, which means that the strength of the resonant Auger decay to the $3s3p^6$ term is overestimated, as we will see later. When these scaling factors are used and the $3s^2 3p^4(^1D)3d\ ^2S$ term is disregarded, the largest error in a term position in the three configurations $3s3p^6$ and $3s^2 3p^4(3d+4s)$ in Ca IV is 0.6 eV.

Similarly if we except $3s^2 3p^4(^1D)3d\ ^2S$, all calculated energy values in Ar II deviate from the observed [32] by less than 0.5 eV relative to the ground state, if the $F^2(3p,3p)$ integral is scaled down to 80%, the $G^k(3p,3d)$ integrals to 55%, and the configuration interaction integrals scaled down to 85%. These scaling factors are slightly different from those used earlier [16], but, since it is important to be able to determine the scaling factors for K as accurately as possible, we have attempted to improve the Ar II values.

Based on the empirical scaling factors, we estimated scaling factors of 82% for $F^2(3p,3p)$, 65% for $G^k(3p,3d)$, and 85% for the configuration interaction integrals in K, assuming that K II is closer to Ar II than to Ca IV. However, it is clear that there is an uncertainty in these values. As a check we have calculated the expected structure of the $3s3p^6+3s^2 3p^4(3d+4s)$ and $3s^2 3p^5+3s^2 3p^4 4p$ configurations in K III as well as the structure of the $3s^2 3p^4$ ground configuration in K IV using these parameters. The K III calculation shows that all the reported 4p levels [29] seem to be correct as well as the 4s levels, except possibly $(^1S)4s\ ^2S$. However, of the reported 3d levels, the $(^1S)3d\ ^2D$ term is incorrectly identified and the $(^1D)3d\ ^2D$ and ^2S terms probably also. The parameter values seem quite accurate—for the 4s and 4p levels there is agreement within about 0.1 eV, except for the $(^1S)4s\ ^2S$ term—while the errors for the 3d terms are

somewhat larger but smaller than 0.5 eV. In the calculation for K IV, which only tests the scaling factor for the $F^2(3p,3p)$ integral, the agreement with the observed energy level values is better than 0.1 eV.

The structure of the Auger spectrum in K is calculated using these scaling factors. This accounts directly for the grand-parent structure of the final states of the Auger process. The correlation among the two outer electrons is taken into account in a first approximation by explicitly including the $4s^2$, $4p^2$, $3d^2$, and $3d4s$ configurations in addition to the use of scaling for these configurations using the same set of scaling factors as for the inner electrons. Overlap integrals are included in the calculation of the configuration interaction as well as the dipole integrals. The necessity for this step is related to the importance of shake processes as discussed in the next section.

For K the Auger decay with continuum f waves is calculated to be about 17 times weaker than the p wave decay in a single-configuration approximation using theoretical transition energies and only the continuum p wave was included in the K and Ca calculations. For Ca the continuum f wave is estimated to be 20 times weaker than the p wave while for Ar the ratio is slightly smaller than for K. For Ar it was found [16] that some final levels, which only can be reached with an f wave, are observed but, except for these few levels, the f wave is only important at the few percent level. Thus we expect that the neglect of the f wave in the K and Ca decays will have a very small effect on the quality of the calculations.

B. Shake probabilities

One important problem encountered is the strength of the shake processes in the three elements. In the case of Ar we have found strong shakeup and shakedown effects but little evidence for shakeoff processes, while Matsuo *et al.* [8] have identified rather strong shakeoff probabilities in K and Ca. For Ar there is good agreement between the observed shakeup and shakedown probabilities and HF calculations of overlap factors. These calculations also predicted that the amount of shakeoff should be limited. We have carried out similar calculations for K and Ca and the results are presented in Table I. The calculations for Ar and K have been carried out using two different HF programs, namely, the approximately relativistic HF code (HFR) due to Cowan and Griffin [26,33] and the nonrelativistic HF code due to Froese Fischer [34] while for Ca only the former results are shown. The differences between the two sets of results are rather large, showing the sensitivity of the d orbitals to the precise details of the screening. However, the calculations agree about the main points. In Ar the $3d$ orbital collapses between the initial state with a $2p$ hole and the final state with two $3p$ holes. The initial $3d$ orbital in Ar is therefore similar to the $4d$ orbital in the final state and the $4d$ orbital in the initial state is nearly orthogonal to the $4d$ orbital in the final state and has its main overlap with $5d$ in agreement with the experimental findings [16]. In both K and Ca, the $3d$ orbital is collapsed in both the initial and final core-hole states with overlaps of 94% and 100%. However, the effect of the collapse on the higher orbitals is rather different and typical for the behavior of an orbital in a double-well potential. When the $3d$ orbital collapses into the inner well, the higher orbitals do not follow but stay partly in the outer well until the inner well deepens further as discussed by Griffin, Andrew, and Cowan [35]. In the present case the initial $4d$ orbital in K has its main overlap with $5d$ and only in Ca is its overlap with $4d$ becoming equal to the overlap with $5d$.

TABLE I. Calculated overlaps (squared) (in percent) between the initial states $2p^5 3s^2 3p^6 4s^k n'd$ and the final states $2p^6 3s^2 3p^4 4s^k nd$ in Ar ($k=0$), K ($k=1$), and Ca ($k=2$) obtained in HF calculations. The right-hand value is obtained using the Cowan (HFR) code [26,33] and the left-hand value using the Froese Fischer HF code [34].

Initial state	Overlap with final $3p^4 nd4s^k$ states (%)									
	$n=3$		$n=4$		$n=5$		$n=6$		$n=7$	
Ar $2p^5 3s^2 3p^6 3d$	32	22.5	60	64.9	6	10.3	0.004	0.001	0.003	0.005
K $2p^5 3s^2 3p^6 3d4s$	95	94.2	3.4	3.4	0.001	0.12				
Ca $2p^5 3s^2 3p^6 3d4s$		99.6		0.04		0.0005				
Ar $2p^5 3s^2 3p^6 4d$	12	10.2	0.04	0.8	63	54.0	24	33.8	0.2	0.5
K $2p^5 3s^2 3p^6 4s4d$	5.6	5.8	41	32.2	53	59.5	0.007	2.5		0.001
Ca $2p^5 3s^2 3p^6 4s^2 4d$				50.6		47.4		0.9		
Ar $2p^5 3s^2 3p^6 5d$	6	6.1	0.8	0.02	8.0	10.8	32	20.1	50	58.5
K $2p^5 3s^2 3p^6 4s6d$	1.6	2.0	9.9	10.1	4.0	0.9	73	69.3	12	12
Ca $2p^5 3s^2 3p^6 4s^2 6d$		0.2		12.1		6.1		70.9		10.6
Ar $2p^5 3s^2 3p^6 6d$	3	2.9	0.7	0.1	1.7	3.3	13	11.2	4.7	0.7
K $2p^5 3s^2 3p^6 4s6d$	0.8	1.0	4.2	4.5	3.2	1.7	3.2	5.9	51	41.6
Ca $2p^5 3s^2 3p^6 4s^2 6d$		0.1		4.8		4.4		2.0		54.1

While this result is very interesting, experimental confirmation is difficult because, when the 3d orbital collapses, the main part of the $2p \rightarrow nd$ oscillator strength becomes associated with the $2p \rightarrow 3d$ transitions and instead of observing a well-developed Rydberg series as in Ar mainly the strong broad 3d transitions are observed which, however, often mask some of the other members in the series. Only weak structures due to higher series members could be detected [7–10]. The data in Table I show that in K and Ca shakeoff as such is predicted to be much smaller than the approximately 10% estimated by Matsuo *et al.* [8], but the predicted shakeup could be important if it leads to a second-step autoionization process becoming possible as observed for example in Ar [36].

C. Branching ratios

For an understanding of the resonant Auger decay, the branching between different final states is very important. In Table II, we show the calculated branching ratios from

TABLE II. Calculated branching ratios in the single-configuration approximation for the resonant Auger decay of the $2p \rightarrow 3d$ resonances in Ar, K, and Ca. Also the average transition energies in the HF approximation are given as well as the possible partial waves connected with the decays. The initial configurations are $2p^5 3s^2 3p^6 3d 4s^k$ with $k=0$, 1, and 2 for Ar, K, and Ca, respectively. The numbers in parentheses in column 4 are the branching ratios from a particular initial level, namely, the higher resonance in Ar and the lower resonance in Ca (see text).

Final configuration	Partial waves	Average energy (eV)	Branching (%)	
$Ar^+ 3s^2 3p^4 3d$	p,f	213	76.7	(76.6)
$3s 3p^5 3d$	s,d	196	22.5	(22.5)
$3s^0 3p^6 3d$	p	175	0.7	(0.7)
$3s^2 3p^5$	s,d,g	232	0.08	(0.08)
$3s 3p^6$	p,f	214	0.01	(0.04)
$K^+ 3s^2 3p^4 3d 4s$	p,f	249	73.8	
$3s 3p^5 3d 4s$	s,d	229	21.1	
$3s^0 3p^6 3d 4s$	p	204	0.8	
$3s^2 3p^5 3d$	s,d	272	0.4	
$3s^2 3p^5 4s$	s,d,g	273	3.3	
$3s 3p^6 3d$	p	250	0.03	
$3s 3p^6 4s$	p,f	251	0.4	
$3s^2 3p^6$	p,f	293	0.01	
$Ca^+ 3s^2 3p^4 3d 4s^2$	p,f	286	71.6	(69.4)
$3s 3p^5 3d 4s^2$	s,d	263	19.9	(19.3)
$3s^0 3p^6 3d 4s^2$	p	235	0.8	(0.8)
$3s^2 3p^5 3d 4s$	s,d	317	1.1	(1.0)
$3s^2 3p^5 4s^2$	s,d,g	315	5.9	(7.1)
$3s 3p^6 3d 4s$	p	292	0.08	(0.08)
$3s 3p^6 4s^2$	p,f	290	0.6	(2.2)
$3s^2 3p^6 3d$	p	342	0.002	(0.002)
$3s^2 3p^6 4s$	p,f	344	0.03	(0.1)

becomes associated with the $2p \rightarrow 3d$ transitions and instead of observing a well-developed Rydberg series as in Ar mainly the strong broad 3d transitions are observed which, however, often mask some of the other members in the series. Only weak structures due to higher series members could be detected [7–10]. The data in Table I show that in K and Ca shakeoff as such is predicted to be much smaller than the approximately 10% estimated by Matsuo *et al.* [8], but the predicted shakeup could be important if it leads to a second-step autoionization process becoming possible as observed for example in Ar [36].

C. Branching ratios

For an understanding of the resonant Auger decay, the branching between different final states is very important. In Table II, we show the calculated branching ratios from the $2p^5 3d 4s^k$ initial configurations in Ar ($k=0$), K ($k=1$), and Ca ($k=2$) to all final states possible in the HF single-configuration approximation for the initial and final states which means that the final configurations can differ by a maximum of two electrons from the initial one. The branching ratios are obtained by summing all decay rates from the initial to each individual final configuration in the HF approximation. This assumes that *all* initial states are populated (statistically) while in practice in Ar and Ca, for example, only two of the three $J=1$ states are populated. In the case of the higher resonance in Ar, $2p^5(^2P_{1/2})3d\,''^3D''$, and the lower resonance in Ca, $2p^5(^2P_{3/2})3d4s^2\,''^3D''$, we give in parentheses the specific branching ratios which show that the difference between the approximate calculation reported in Table II and the correct one probably is less than the error introduced by the use of the single-configuration approximation. The reason is that the prominent decays have the 3d electron as a spectator. When this is the case, the summed decay rate (although not the rates to particular final states) is independent of the initial state and it makes thus no difference for the branching whether the total rate is considered or the rate from a particular initial state. Only for those decays, where the 3d electron participates, do the initial state influence the branching and these are the weaker decays as can be seen from Table II, which also shows that, as expected, the main differences are found for these decays.

For Ar, Aksela *et al.* [17] have published similar branching ratios using Dirac-Fock calculations with configuration interaction between the final ionic configurations included. This means that the branching between $3s 3p^6$ and $3s^2 3p^4 3d$ was not determined, but when our values for these two decays are added together there is agreement with their values to within 2% in all cases.

IV. RESULTS AND DISCUSSION

A. Ar: Ground state $1s^2 2s^2 2p^6 3s^2 3p^6\ ^1S^o$

In the 2p excitation region, the absorption spectrum of Ar [5] is dominated by series of strong discrete resonances just below the 2p thresholds, $Ar^+ 2p^5(^2P_{3/2})3s^2 3p^6$: $E_B = 248.63$ eV and $2p^5(^2P_{1/2})3s^2 3p^6$:

$E_B = 250.78$ eV [37]. The resonances are assigned to the Ar* $2p^5(^2P_{3/2},^2P_{1/2})ms,nd$ ($m = 4,5,\ldots$; $n = 3,4,\ldots$) Rydberg series. According to ion-yield spectra [6] the main part ($\approx 70\%$) of the oscillator strengths for the lowest of these transitions ($2p \rightarrow 4s$) is contained in the cross section for the generation of singly charged ions. This result is corroborated by photoelectron spectra taken at the Ar $2p \rightarrow ms,nd$ resonances [14,16], which show that the main intensity in the electron spectra is due to autoionization into final states with a double vacancy in the $3p$ shell, i.e., Ar* $2p^5ms,nd \rightarrow Ar^+$ $2p^63s^23p^4ms$, $nd + \epsilon l$ in agreement with the branching ratios in Table II. For low values of m and n these Ar^+ levels are lying below the threshold of the lowest Ar^{2+} continuum and thus a subsequent decay is only possible via fluorescence except in special cases where shakeup is important [36]. Therefore the electron lines found in the low-kinetic-energy region of the spectra emitted upon the decay of the Ar $2p$ resonances [25,38] must be due to second-step decays such as Ar^+ $3s^13p^5ms,nd \rightarrow Ar^{2+}$ $3s^23p^4 + \epsilon l$ in combination with shake processes. These two-step decay channels, monitored, for example, by the number of Ar^{2+} ions, comprise only about 20% of the total oscillator strength, which is in agreement with the calculated branching in Table II, and they will not be discussed further.

The first measurements [14] of the main part of the electron spectrum emitted upon the decay of the Ar* $2p^5(^2P_{3/2})3d$ resonance at $\hbar\omega = 246.9$ eV already demonstrated the importance of the shakeup processes arising from the different degree of collapse of the $3d$ wave function in the initial excited $2p$ state compared to the final ionic state. In a recent publication [16] we described in some detail the special properties of the $3d$ wave function which leads to a high shakeup probability as well as a very complex multiplet structure for the Ar^+ $3p^43d$ configuration. The interpretation was based on spectra excited on the Ar* $2p^5(^2P_{3/2})3d$ and Ar* $2p^5(^2P_{3/2})4d$ resonances in combination with extensive calculations of the shakeup probabilities and of the individual Auger decay rates. The most striking result of this investigation was the nearly complete suppression of the direct transition Ar* $2p^54d \rightarrow Ar^+$ $3p^44d$, about 90% of the total decay rate going into shake processes, as mentioned already. A similar situation has recently been observed by Whitfield, Caldwell, and Krause [39] for $2p \rightarrow ms,nd$ excitations in Mg. The observations are both for Ar [16] and for Mg [39,40], in agreement with simple shake calculations which for Ar (Table I) show practically no intensity for the direct $4d \rightarrow 4d$ transition.

In Fig. 2 the electron spectra emitted upon the decay of the Ar* $2p^5(^2P_{3/2})4s$ [Fig. 2(a)] and Ar* $2p^5(^2P_{1/2})4s$ [Fig. 2(b)] resonances are displayed. Besides the Ar^+ $3s^13p^6\ ^2S$ photoline ($E_B = 29.24$ eV [32]) the dominant lines are due to the Ar* $2p^54s \rightarrow Ar^+$ $2p^63s^23p^4(4s$ or $5s) + \epsilon l$ decay. Small contributions arise from the $L_{23}M_{23}M_{23}$ Auger transitions induced by the second-order light of the monochromator (indicated by the dotted lines). For the Ar* $2p^5(^2P_{1/2})4s$ resonance [Fig. 2(b)] additional structures are caused by the decay of the very strong Ar* $2p^5(^2P_{3/2})3d$ resonance, which is located so near that it is excited to some extent due to the bandpass ($\Delta\hbar\omega = 0.6$ eV) of the monochromator.

The difference in the intensity ratio $I(^2P):I(^4P)$ of the $Ar^+3p^4(^3P)4s$ final state in the spectra corresponding to the Ar* $2p^5(^2P_{3/2})4s$ and the Ar* $2p^5(^2P_{1/2})4s$ resonance, respectively, which is clearly visible in Fig. 2, has already been discussed briefly elsewhere [41,42]. In LS coupling, the two resonances would be labeled ^1P [Fig. 2(a)] and ^3P [Fig. 2(b)], respectively, where the latter is observed due to the spin-orbit mixing that gives ^1P character to both levels. The first calculations using a single configuration approach reproduced the relative intensities quite well (Table III, calc. a). The results of a more extensive calculation including the mixing with the $3p^43d$ final states are given in Table III (calc. b). These results show only small changes with respect to the terms built on $3p^4(^3P)$ and (^1S) parent terms, but predict a partition of the intensity of the line with $3p^4$ (^1D) character into two, i.e., the mixed states Ar^+ $3p^4(^1D)4s\ ^2D$ and Ar^+ $3p^4(^1D/^3P)3d\ ^2D$ [16].

In the experiment (Fig. 2) the resolution was not high enough to allow an unambiguous corroboration of this prediction. However, a small shift of about 0.1 eV towards higher binding energies of the ^2D line relative to the other $3p^44s$ components is observed as well as a slightly broader total line width (about 0.5 eV for ^2D compared to about 0.4 eV for ^2S, ^2P, and ^4P). For a more stringent experimental test higher resolution would be necessary.

It is interesting to note that in relativistic multichannel calculations for the normal Auger decay of the $2p$ hole in

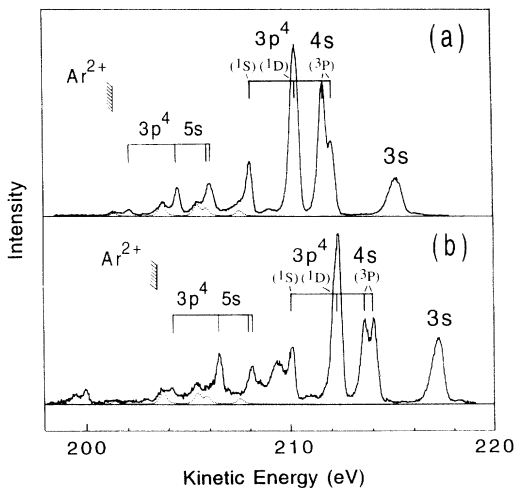

FIG. 2. Electron spectra of atomic Ar photoexcited at (a) the Ar* $2p^5(^2P_{3/2})3s^23p^64s\ ''^1P''$ ($\hbar\omega = 244.4$ eV) and (b) the Ar* $2p^5(^2P_{1/2})3s^23p^64s\ ''^3P''$ ($\hbar\omega = 246.5$ eV) resonances, respectively ($\Delta\hbar\omega = 0.6$ eV; $U_{ret} = 200$ V). The $L_{23}M_{23}M_{23}$ Auger transitions induced by the second-order light of the monochromator are given by dotted lines. The Auger $L_{23}M_{23}M_{23}$ spectrum was measured separately at $\hbar\omega = 270$ eV. For the $3p^44s$ configuration, the parent terms in the $3p^4$ configuration, ^1S, ^1D, and ^3P are indicated as well as the splitting of the latter in a ^2P and a ^4P term by the interaction with $4s$.

TABLE III. Comparison between experimental and calculated relative transition probabilities (in percent) for Ar* $2p^5(^2P_{3/2})3s^23p^64s\,''^1P''\rightarrow Ar^+\ 2p^63s^23p^44s,3d$ and Ar* $2p^5(^2P_{1/2})3s^23p^64s\,''^3P''\rightarrow Ar^+\ 2p^63s^23p^44s,3d$. The two calculations are described in the text. The binding energy is from Minnhagen [32]; for the labels see Ref. [16].

		Intensity					
			Initial state				
$3p^4(4s+3d)$ Final state	Binding energy (eV)		$2p^53s^23p^64s\ ^1P$			$2p^53s^23p^64s\ ^3P$	
		Expt.	Calc. *a*	Calc. *b*	Expt.	Calc. *a*	Calc. *b*
$3p^4(^3P)4s\ ^4P$	32.50	13	18	20	19	25	24
$3p^4(^3P)4s\ ^2P$	32.95	29	32	31	19	21	22
$3p^4(^1D/^3P)3d\ ^2D$	34.20			25			25
		46	40		53	43	
$3p^4(^1D)4s\ ^2D$	34.46			15			18
$3p^4(^1S)4s\ ^2S$	36.50	12	10	9	9	11	11

Ar, Tulkki *et al.* [43] have obtained branching ratios between the three final $3p^4SL$ terms which show similar deficiencies as those in Table III, namely, an overestimate of the decay rate to the ^3P and an underestimate of the rate to the ^1D term.

B. K: Ground state $1s^22s^22p^63s^23p^64s\ ^2S_{1/2}$

In contrast to Ar, the $2p$ excitation spectrum of K shows no well-developed Rydberg series corresponding to the Ar* $2p^5ms,nd$ series. The main part of the K $2p$ oscillator strength is concentrated in $2p\rightarrow 3d$ excitations. The absorption spectrum [7] as well as the ion-yield spectra [8,9] are dominated by two strong resonances which Mansfield [7] assigned to the K* $2p^5(^2P_{3/2},^2P_{1/2})3d4s$ excited states split by the spin-orbit interaction of the $2p$ hole. The partial collapse of the $3d$ wave function in the $2p$ excited state, caused by the increased charge of the core, which is not fully screened by the $4s$ electron, gives rise to the strength of the $2p\rightarrow 3d$ transitions. We discuss below that with the available photon-energy resolution the higher resonance appears to be composed of several states of different types. However, for simplicity we retain the labels given to the two resonances above.

The electron spectrum emitted upon the decay of the K* $2p^5(^2P_{3/2})3d4s$ resonance has already briefly been discussed in the introduction demonstrating the complexity of the decay mechanisms and the large number of decay channels for this resonance. Figure 3 displays four autoionization spectra measured by tuning the monochromator to the energies of the two strong resonances (K* $2p^5(^2P_{3/2})3d4s$ [Fig. 3(b)] and (nominally) K* $2p^5(^2P_{1/2})3d4s$ [Fig. 3(c)]) and to photon energies below ($\hbar\omega=291$ eV [Fig. 3(a)]) and well above ($\hbar\omega=310.5$ eV [Fig. 3(d)]) these resonances and the $2p$ thresholds. The intensities of the spectra are adjusted relative to each other via the partial cross section of the $3p$ photoline, which was measured separately (see below, Sec. V). For the spectra emitted upon the decay of the $2p\rightarrow 3d$ resonances, the strong enhancement of the main $3s$ and $3p$ photolines and of the lines in the region 200 eV $<E_{kin}<255$ eV clearly shows up. The most intense lines (240 eV $<E_{kin}<255$ eV) are the resonant Auger transitions assigned to the decay K* $2p^53d4s\rightarrow K^+\ 2p^63s^23p^43d4s+\epsilon l$. The main part of the weaker structures at the low-kinetic-energy side of these lines are probably due to autoionization into states belonging to the $K^+\ 3s^13p^53d4s$ configuration as predicted by the branching ratios in Table II while according to Table I shakeup transitions are expected to make a minor contribution. Figure 3(d) shows the normal L_{23} Auger spectrum with the dominating $L_{23}M_{23}M_{23}$ lines, excited at a photon energy $\hbar\omega=310.5$ eV, i.e., well above

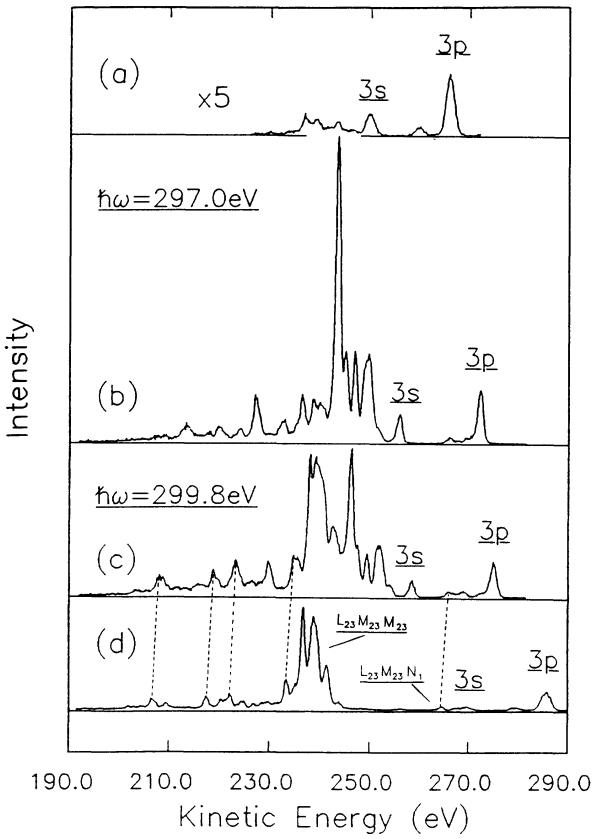

FIG. 3. Electron spectra of atomic K photoexcited at (a) $\hbar\omega=291$ eV; (b) $\hbar\omega=297.0$ eV, i.e., the K* $2p^5(^2P_{3/2})3s^23p^63d4s$ resonance; (c) $\hbar\omega=299.8$ eV, i.e., the (nominal) K* $2p^5(^2P_{1/2})3s^23p^63d4s$ resonance (see text); and (d) $\hbar\omega=310.5$ eV. ($\Delta\hbar\omega=1.0$ eV; $U_{ret}=150$ V.) The relative intensities are normalized via the $3p$ cross section shown in Fig. 12(b).

the $2p$ thresholds [K^+ $2p^5(^2P_{3/2})4s$: $E_B=300.2$ eV and $2p^5(^2P_{1/2})4s$: $E_B=303.1$ eV [7]]. This photoexcited Auger spectrum resembles the well-known and extensively studied spectra excited by electron bombardment [44,45]. There are no obvious similarities between the $3p^4 4s$ multiplet, which determines the structure of the normal $L_{23}M_{23}M_{23}$ Auger spectrum [Fig. 3(d)], and the $3p^4 3d 4s$ multiplet of the "resonant Auger spectrum" [Figs. 3(b) and 3(c)]. Caused by the collapse of the $3d$ wave function in the K^+ $3p^4 3d 4s$ final states, the resulting $3p \leftrightarrow 3d$ interaction masks the $3p^4(^1S, ^1D, ^3P)$ "parent" structure and gives rise to a very complex multiplet, while in the case of K^{2+} $3p^4 4s$ the $3p \leftrightarrow 4s$ interaction is small and the $3p^4$ parent distribution is basically preserved except for a small splitting of the ^3P line seen in high-resolution spectra [44,45]. This is similar to the situation in Ar and Ca and it means that the spectator model fails completely for the interpretation of the decay spectrum of the K* $2p^5 3d 4s$ resonances, as it does for the $2p \rightarrow 3d$ resonances in the neighboring elements [16,19].

Since no experimental data concerning the energies of the K^+ $3p^4 3d 4s$ final states exist, and since we, as mentioned, have found that some of the tabulated energy values of the K^{2+} $3p^4 3d$ configuration [29] are erroneous, calculations of excitation and decay spectra are essential. Mansfield [7] has published an interpretation of the absorption features based on HF calculations without including configuration interaction. He used the jK coupling scheme and due to the strength of the spin-orbit coupling for the $2p$ electron, the total angular momentum j of this electron is clearly a good quantum number. However, for the coupling of the two outer electrons the LS scheme is probably preferable, and we have used intermediate coupling with LS basis states including configuration interaction.

In LS coupling, there are only two states in the $2p^5 nd 4s$ configurations that can be reached from the ground state by an electric dipole transition, namely, the $J=\frac{1}{2}, \frac{3}{2}$ levels belonging to the $2p^5 nd\,(^1P)4s\ ^2P$ term if the nd electron is coupled more strongly to the $2p$ core than to the $4s$ electron (and spin-orbit interaction weak). The two $2p^5 nd\,(^3P)4s\ ^2P$ levels cannot be reached by a dipole transition in this approximation. We find good agreement between the 297.0-eV resonance and the two levels belonging to the $2p^5 3d\,(^1P)4s\ ^2P$ term predicted around 297.25 eV with a splitting of 0.02 eV. The levels are, however, only about 50% pure in the LS-coupling scheme and the remaining oscillator strength is distributed over a somewhat larger number of levels around 300 eV in good agreement with the position of the other strong absorption feature observed [7]. In particular, the recent ion-yield spectrum [9] shows clearly that the feature at higher energy is composed of a number of individual peaks. Comparing with this spectrum, the calculations predict correctly that the higher resonance is considerably weaker than the lower one but, since the higher resonance has a composite structure, the ratio between the intensities of the two peaks cannot be compared to the statistical ratio 2:1. The 3-eV splitting is due to the spin-orbit splitting of the $2p$ hole, which causes the breakdown of the LS-coupling scheme. The two levels of the $2p^5 4s^2\ ^2P$ term are split for the same reason and the $J=\frac{3}{2}$ level is predicted just below 295 eV, but has very little oscillator strength associated with it in agreement with the experimental findings [7], while the $J=\frac{1}{2}$ level is predicted somewhat above the 297.0-eV resonance and not observed either. The transitions to other $2p^5 4sms$ states are predicted to be weaker still. One significant difference between the interpretation of the absorption spectrum [7] and the present interpretation concerns the weak features, which Mansfield ascribed to excitations to $2p^5 3dms$ in favor of $2p^5 4snd$. The former transitions are forbidden in the single-configuration approximation and Mansfield proposed that they could be due to the mixing between $3d$ and $4s$ which he did not include in his calculations. These interactions are included here and we find that the transitions to $2p^5 3d 5s$ are likely to be masked and that the weak observed features [7,9] probably are due to $4snd (n \geq 4)$. In the $2p^5 4s 4d$ configuration the coupling between $4s$ and $4d$ is stronger than the coupling between, for example, $4d$ and $2p^5$, thus dividing the oscillator strength over a larger number of individual levels. However, the lowest $4d$ resonance(s) is predicted about 0.4 eV below the second strong resonance and as discussed later we find evidence for a resonance in this region as well as for its spin-orbit split partner at higher energy. As consequence of the complicated excitation spectrum for the 300-eV resonance we have attempted a quantitative identification of the Auger decay spectrum of the 297.0-eV resonance only.

A comparison between the spectra emitted upon the decay of the K* $2p^5(^2P_{3/2})3d 4s$ and K* $2p^5(^2P_{1/2})3d 4s$ resonances [Figs. 3(b) and 3(c)] shows large differences with respect to the relative intensity distribution within the kinetic-energy region tentatively assigned to the K^+ $3p^4 3d 4s$ multiplet. Taking into account a relative shift of $\Delta E_{\text{kin}}=2.8$ eV due to the different excitation energies and the difference between the integrated intensities due to the difference in oscillator strength between the two resonances, there is additional intensity at $E_{\text{kin}}<245$ eV in the spectrum taken at $\hbar\omega=299.8$ eV. However, part of it stems from the normal L_3 Auger spectrum. The lowest $2p$ threshold is only 0.5 eV above the energy of the nominal $2p^5(^2P_{1/2})3d 4s$ resonance and due to the monochromator bandpass of $\Delta\hbar\omega \cong 1.0$ eV, direct ionization is taking place to some degree. The near-threshold $2p$ ionization causes a shift in the kinetic energy of the corresponding L_3 Auger lines induced by the well-known post-collision interaction (PCI) effect (e.g., [46–48]). The shift is indicated by the dashed lines, which connect some peaks of the Auger spectrum [Fig. 3(d)] with their possible counterparts in the resonant spectrum [Fig. 3(c)]. From that we estimated a PCI shift of $\Delta E<0.8$ eV.

In order to put our interpretation on a firm basis we recorded a series of electron spectra excited at various photon energies in the region of the $2p$ resonances and $2p$ thresholds. These spectra are displayed in Fig. 4. For orientation, the K^+ $3s 3p^6 4s$ photoline, which is calculated to be more than 10 times as likely as final state as K^+ $3s 3p^6 3d$ (Table II), is indicated at $E_B(3s)=41.0$ eV. In this representation the similarities between the two reso-

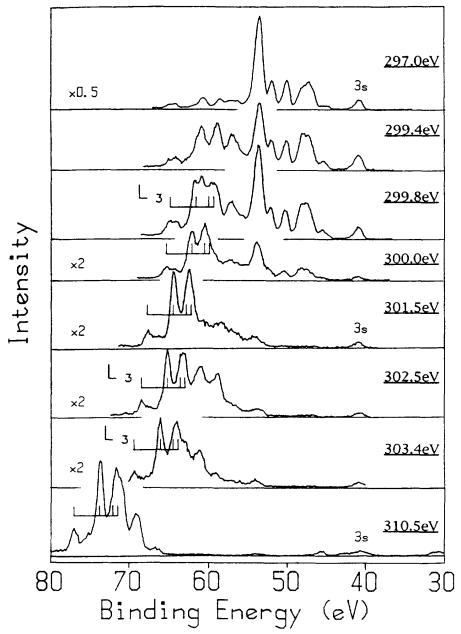

FIG. 4. Electron spectra of atomic K photoexcited at the photon energies indicated in each panel. The relative intensities of the spectra are normalized via the $3p$ cross sections (the $3p$ photoline is not shown in the figure). ($\Delta\hbar\omega=1.0$ eV; $U_{\text{ret}}=150$ V.)

nantly excited spectra at $\hbar\omega=297.0$ and 299.8 eV in the region $E_B \leq 55$ eV as well as the discrepancies for $E_B > 55$ eV are quite obvious. The lines arising from the L_3 Auger decay are marked with vertical bars. Figure 4 supports the assignment of part of the structure at 55 eV $< E_B <$ 65 eV in the spectrum taken at $\hbar\omega=299.8$ eV to L_3 Auger transitions. But additional intensity remains, which clearly shows up as discrete lines in the spectrum taken at $\hbar\omega=299.4$ eV. These lines, at least the two lines at $E_B=58.6$ and 60.9 eV, seem to reappear at $\hbar\omega=302.5$ eV, i.e., they behave like resonant autoionization lines. Based on these findings we conclude that the electron spectrum emitted upon the decay of the K* $2p^5(^2P_{1/2})3d4s$ resonance comprises contributions from the L_3 Auger decay and from the decay of another K* $2p^5(^2P_{3/2})nln'l'$ resonance located close to 299.4 eV and identified as $nln'l'=4s4d$ on the basis of the calculations. According to this interpretation the decay of the K* $2p^5(^2P_{1/2})4s4d$ spin-orbit partner causes the extra lines in the spectrum taken at $\hbar\omega=302.5$ eV.

This interpretation is corroborated by results obtained at low kinetic energies. In Fig. 5 three spectra are displayed in the region 5 eV $\leq E_{\text{kin}} \leq$ 35 eV comprising all observed lines in this part of the electron spectrum. Upon excitation of the $2p \rightarrow 3d$ resonances [Figs. 5(a) and 5(b)] a considerable fraction of the intensity can be ascribed to second-step decays, i.e., mainly K^+ $3p^4 3d4s \rightarrow K^{2+}$ $3p^5+\epsilon l$. With respect to the energy axis the second-step Auger lines form a mirror image of the first-step autoionization lines displayed in Figs. 3(b) and 3(c). The "reflected autoionization spectra" are given by the dashed lines in Figs. 5(a) and 5(b). The $3s$ photoline is again indicated for orientation and is situated at $E_{\text{kin}}=5$ eV. For the spectrum recorded at $\hbar\omega=297.1$ eV, the low-kinetic-energy lines nicely reproduce most of the structure of the reflected autoionization spectrum. The small bandpass of the electron analyzer at low kinetic energies allows us to resolve the splitting of the strongest line at $E_{\text{kin}} \simeq 18$ eV, which is due to the spin-orbit splitting of the K^+ $3p^5\,^2P$ term. The many lines around $E_{\text{kin}}=12$ eV in the low-energy spectrum reflect the large number of autoionizing transitions responsible for the broad maximum at $E_B=48$ eV in Fig. 4.

Turning now to the spectra recorded at $\hbar\omega=299.8$ eV [Fig. 5(b)] we find for kinetic energies *below* 19 eV the same type of agreement between the second-step Auger lines and the reflected autoionization spectrum as encountered above. However, for kinetic energies *above* 19 eV the reflected autoionization spectrum by far overshoots the second-step Auger spectrum. This is consistent with the interpretation proposed above, since most of the extra intensity in the reflected spectrum can be ascribed to the normal Auger decay K^+ $2p^5(^2P_{3/2})4s \rightarrow K^{2+}$ $2p^6 3s^2 3p^4 4s+\epsilon l$. The final K^{2+} states in this de-

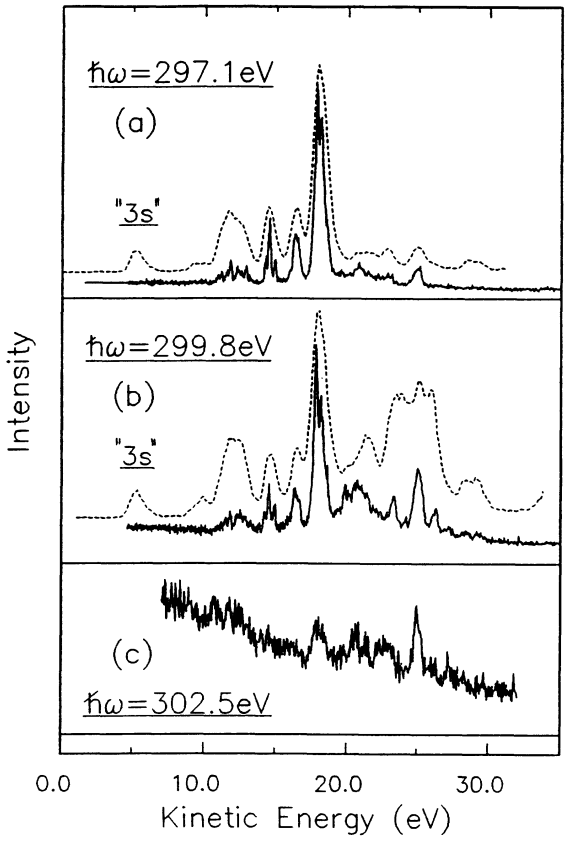

FIG. 5. Second-step Auger spectra of atomic K (solid line) photoexcited at three different photon energies (a) $\hbar\omega=297.1$ eV, (b) $\hbar\omega=299.8$ eV, and (c) $\hbar\omega=302.5$ eV. The dashed lines represent the corresponding first-step autoionization spectra projected on the low-kinetic-energy region as described in the text. ($\Delta\hbar\omega=1.0$ eV; $\Delta E_{\text{kin}}=0.008E_{\text{kin}}$.)

cay are located below the lowest K^{3+} states and therefore cannot undergo a second-step decay. However, in comparison to the low-energy spectrum taken at 297.1 eV [Fig. 5(a)] the spectrum recorded at 299.8 eV [Fig. 5(b)] displays some strikingly strong lines for kinetic energies above 19 eV. These lines are also present in the low-energy spectrum taken at a photon energy of 302.5 eV [Fig. 5(c)]. This supports the assumption that there exist two spin-orbit split K* $2p^5 4s4d$ resonances close to 299.4 and 302.5 eV for which the two-step decay contributes to the electron spectra. The recent high-resolution ion spectra reported by Kanno *et al.* [9] show a marked peak at about 302.4 eV and a strong, clearly asymmetric line, centered at 299.8 eV, indicating the existence of several resonances in the region of the nominal $2p^5(^2P_{1/2})3d4s$ resonance. As mentioned, our calculations predict the presence of a $2p^5(^2P_{3/2})4s4d$ resonance about 0.4 eV below the 299.8-eV resonance with a spin-orbit split partner at about 302.3 eV, in good agreement with this interpretation. These resonances, in particular the lower one, are calculated to be weak, but they are in the right position to explain the experimental findings. In Sec. III B we noted that in K the $4d$ orbital collapses between the initial and final state of the Auger process which could explain the many lines observed in the low-energy (second-step) Auger spectrum. Another contributing factor is the fact that we predict the 299.8-eV resonance to correspond to a fairly large number of initial states.

In Fig. 6 we present the calculated and observed Auger spectra for the 297.0-eV resonance. The initial states were obtained from the CI expansion used to calculate the excitation spectrum including the

$$2p^5 3s^2 3p^6(3d4s+4d4s+5d4s+3d5s+4s^2+4s5s+4s6s+3d^2+3d4d+4p^2+4p5p)+2p^6 3s^2 3p^5(3d4s+4s^2)$$

configurations and the final states are based on a CI expansion including the

$$2p^6 3s^2 3p^4(3d4s+4s^2+3d^2)+2p^6 3s 3p^6(3d+4s)$$

configurations coupled to a continuum p electron and using the scaling factors discussed in Sec. III A to determine the structure of the ionic states. A free electron energy of 245 eV was used for the calculation of all the transitions. The decays involving two $3p$ electrons are 100 times or more likely than a decay involving a $4s$ electron (Table II). Similarly the $3s3p^64s$ final states are 10 times more likely than the $3s3p^63d$ states. On the other hand, configuration interaction in the final state is rather strong which means that some $2p^6 3s^2 3p^4 3d^2$ final states, which cannot be reached in a single-configuration approximation, are calculated to have appreciable strength. The calculated spectrum is a superposition of two spectra corresponding to the two initial $J=\frac{1}{2}$ and $\frac{3}{2}$ levels being populated in the ratio 1:2 as predicted in the calculation of the excitation spectrum. In the calculated spectrum [Fig. 6(b)] a Gaussian spectrometer function with a full width at half maximum (FWHM) of 0.8 eV is used convoluted with a Lorentzian with FWHM of 0.5 eV, which represents the natural linewidth (see Sec. V).

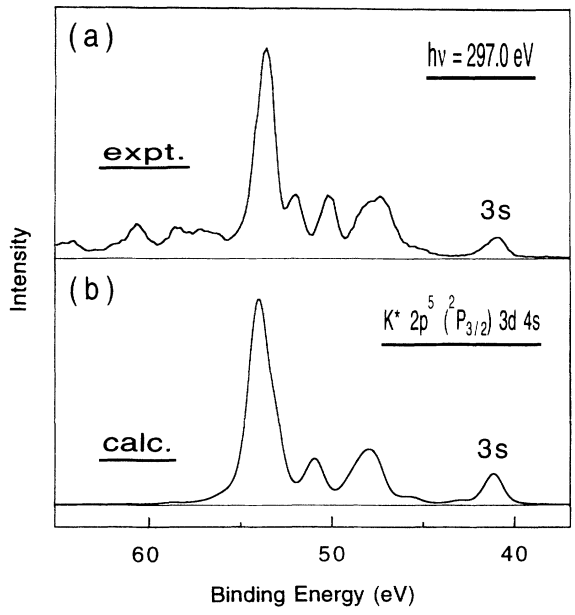

FIG. 6. (a) Observed and (b) calculated Auger spectra for the decay of the K $2p^5(^2P_{3/2})3s^2 3p^6 3d4s$ resonance. The theoretical spectrum is a sum of two spectra as explained in the text.

Figure 6 shows that there is good agreement between the observed and the calculated Auger spectra except that the observed structure at 52 eV is present only as a shoulder in the calculated spectrum which could be due to the scaling factors being slightly wrong. Taking this difference into account, the intensity distribution in the calculated spectrum is in good agreement with the observed except that the strength of the $3s$ peak is overestimated. The same was found in the case of the resonant Auger spectra in Ar [16] and is, as mentioned earlier, ascribed to the fact that the interaction between $3s3p^64s$ and $3s^23p^43d4s$ is used to model the interaction with the whole $3s^23p^44snd/\epsilon d$ series which lead to an overestimate of the $3d$ component in the $3s3p^64s$ term. It turns out that this assumption can be tested in a more quantitative manner.

Table IV shows a detailed comparison for the 297.0-eV resonance. The experimental spectrum [Fig. 6(a)] has been fitted with a total of nine Voigt profiles leading to the energies and intensities given in column 1. Here the intensities have been normalized to 100 for the line at 41.0 eV that is identified as corresponding to the $3s$ hole state: $3s3p^64s$. Column 2 give the equivalent information based on the calculations with the energies calibrated on the 41.0-eV line. The calculated energies have been obtained by fitting the theoretical spectrum in Fig. 6(b) in the same way as the observed. The largest difference be-

TABLE IV. Fitted and calculated binding energies and intensities of the K structures in the decay of the 297.0-eV resonance. The fitted values are obtained by approximating the spectrum displayed in Fig. 6(a) by a superposition of Voigt profiles and the calculated by applying the same procedure to the theoretical spectrum [Fig. 6(b)]. The intensities are normalized to 100 for the line at 41.0 eV, which is identified with decay to the 3s hole state. The percentages for the fitted spectrum are obtained by assuming that the intensity above 53.5 eV contributes only 1.9% (the calculated value for the $3p^4 3d4s$ final configuration) of the total.

Fitted			Calculated		
E_B (eV)	Int.	%	E_B (eV)	Int.	%
41.0	100	a	41.0	100	a
45.0	53	2.7	45.6	20	1.6
47.1	427	21.6	47.9	262	20.0
49.8	250	12.7	50.8	140	10.7
51.5	239	12.1	53.0	196	15.0
53.5	967	49.0	54.0	664	50.8
56.5	131	(1.6)[b]	56.0	21	1.6
58.2	135	(0.3)[b]	58.7	4	0.3
60.3	146	(0.0)[b]			

[a]This line is not included; see text.

[b]Estimated value. The rest of the intensity is believed to be due to, in particular, the $3s3p^5 3d4s$ configuration; see text.

tween observed and calculated energies is 1.5 eV, which is in reasonable agreement with the expected accuracy since both observed and calculated features consists of several transitions and there is no guarantee that the same transitions are involved.

The calculated spectrum has very little intensity above 53.5-eV binding energy while the observed spectrum shows appreciable intensity in this region. We believe that this is due to the decay to the $3s3p^5 3d4s$ configuration, which is not included in the calculated spectrum but according to Table II should account for 21% of the total number of decays and is predicted to lie higher than $3s^2 3p^4 3d4s$. In fact 17% of the fitted intensity is found in this region in good agreement with this prediction. Comparing the calculated and the observed intensities, it can be seen that the calculated intensities systematically are smaller than the observed. This can be understood from the fact that the 3s peak, which is used to normalize the spectrum, is overestimated in the calculation. The calculated percentage distribution shows that in fact the intensity distribution within the $3s^2 3p^4 3d4s$ configuration is predicted very well. These numbers are obtained by calculating the percentage intensity distribution over the $3s^2 3p^4 3d4s$ configuration assuming that the levels above 53.5-eV binding energy in this configuration contribute 1.9% (the calculated value) of the total intensity in this energy region. In this way the influence of the normalization on the 3s peak has been removed and the good agreement between the observed and calculated percentage distributions confirms that the main deficiency of the calculations is the overestimate of the intensity of the 3s peak.

The calculated excitation spectrum predicts that the 299.8-eV resonance is due to a rather large number of initial states. It is thus difficult to predict the subsequent Auger spectrum. However, one important initial state is the $2p^5 3d(^1P)4s\ ^2P$ term (in *LS* coupling) and this state does lead to an Auger spectrum which is rather similar to that predicted for the lower resonance. This is in contrast to the situation for Ca, as we will see shortly, but in agreement with the observed spectra, if we, as discussed above, assume that there is a second resonance excited at 299.4 eV, which contributes also at 299.8 eV due to the 1-eV bandwidth of the photon beam. However, there is another prominent contribution to the 299.8-eV resonance, which has $2p^5 3d4d$ as its main eigenvector component and does lead to a somewhat different Auger spectrum. For example a fairly strong transition is predicted to a level at 58.8 eV close to the observed structure at 58.6 eV (Fig. 4).

Matsuo *et al.* [8] have published results for the ion fractions at the resonances as well as above the 2p thresholds with a resolution of 1.5 eV at threshold for both K and Ca. For the resonant spectrum, Matsuo *et al.* [8] concluded that despite the breakdown of the spectator model for the structure of the Auger spectrum, the model seems to work fairly well for the ion fractions. This is because the main effect of the spectator electron when it interacts with the core is a redistribution of the total decay rate more than a change in the latter. Table II gives the branching ratios (74:21:3:1) between the final configurations $3s^2 3p^4 3d4s, 3s3p^5 3d4s, 3s^2 3p^5 4s$, and $3s^0 3p^6 3d4s$ while all other possible final states are very unlikely. This should be compared to the observed ratios (75:21:2:2) corresponding to the final states $3s^2 3p^4 4s$, $3s3p^5 4s$, $3s^2 3p^5$, and $3s^0 3p^6 4s$ for the decay of the 2p hole in the ion [44]. Thus the relative decay rates are hardly changed by the presence of the 3d electron and, except if the effects of configuration interaction are significantly different in the presence of the 3d electron, the redistribution of Auger rates will not significantly change the total rate per energy interval that determines the ion fraction.

At the $2p \rightarrow 3d$ resonances Matsuo *et al.* [8] concluded that the spectator model gives good agreement for the ion fractions in Ca, but for K they noted that about 10% of the ions have been shifted to the next higher ionization stage with respect to their estimates of the consequences of the spectator model. Matsuo *et al.* [8] attributed this effect to shake processes. However, a 10% effect is larger than predicted by the calculations of overlap integrals in Table I. It is somewhat surprising that the production of K^{3+} ions is the same at the two K resonances since we expect the upper one to have a rather different character from the lower one. In particular the upper resonance is believed to contain a 4d component, which according to Table I would have considerable shakeup associated with it that could lead to production of additional K^{3+} ions at this resonance.

In conclusion, the results suggest that the autoionization spectra emitted upon the decay of the K* $2p^5(^2P_{3/2})3d4s$ and nominal K* $2p^5(^2P_{1/2})3d4s$ resonances are, despite their different composition, rather similar and the observed differences (cf. Figs. 3 and 4) arise mainly from additional line structures superimposed on the spectrum of the $^2P_{1/2}$ resonance. This is rather

different from the situation in Ca which we will turn to now.

C. Ca: Ground state $1s^2 2s^2 2p^6 3s^2 3p^6 4s^2\ {}^1S_0$

The Ca atom is one of the key elements for the understanding of many-electron dynamics in atoms. The sensitivity of the $3d$ orbital to its environment and particularly the collapse of the $3d$ wave function upon excitation of an outer $3p$ or $4s$ electron is well established by several experimental (e.g., [49–52]) and theoretical (e.g., [53–57]) investigations. In addition the elaborate study of the L Auger spectra excited by electron bombardment [58] and the first results for the autoionization of the strong Ca* $2p^5 3d 4s^2$ core resonances [19] demonstrate the important role of the $3d$ wave function also in the case of $2p$ excitations. For the interpretation of the line structures of the Auger and autoionization spectra a strong mixing as well in the initial as in the final state had to be taken into account. In the $2p$ absorption spectrum [10] and the ion-yield spectra [8,9] a further consequence of the $3d$ collapse shows up. Due to the strong $2p$-$3d$ overlap most of the $2p \rightarrow d$ oscillator strength is concentrated in two prominent lines, which are identified as the Ca* $2p^5(^2P_{3/2})3d4s^2$ and Ca* $2p^5(^2P_{1/2})3d4s^2$ resonances, respectively. The high Ca^{2+} and Ca^{3+} yields lead to the expectation that, like in the case of K, second-step Auger decays will manifest themselves in the low-kinetic-energy region of the electron spectra.

In the following we present a more complete version of our earlier work [19] on the autoionization spectra emitted upon the decay of the $2p \rightarrow 3d$ resonances including an investigation of the second-step Auger spectra. In Fig. 7 we show four electron spectra of atomic Ca photoexcited at different photon energies. At $\hbar\omega = 344.2$ eV [Fig. 7(a)], i.e., below the $2p$ resonances and $2p$ thresholds, direct ionization of the outer subshells determines the spectrum. This results in the Ca^+ $3p^5 4s^2$ and Ca^+ $3s^1 3p^6 4s^2$ photolines at $E_B = 34.4$ and 53.1 eV [52], respectively, and in small satellite structures. In analogy with the spectrum of the $3s$ satellites in atomic Ar (e.g., [31,48]) the strongest peak at $E_B = 70.3 \pm 0.5$ eV can be assigned to the Ca^+ $3s^2 3p^4(^1D)3d4s^2\,{}^2S$ final state, which gets its intensity from a strong mixing with the $3s$ main line. Nearly the same intensities for these direct processes are found in the other "off"-resonance spectrum [Fig. 7(d)] recorded at a photon energy of $\hbar\omega = 370.0$ eV. This energy is well above those of the $2p \rightarrow 3d$ resonances and above the Ca^+ $2p^5 3s^2 3p^6 4s^2$ thresholds [10]. The most intense structures are L Auger lines, particularly $L_{23}M_{23}M_{23}$ and $L_{23}M_{23}N_1$ lines. At this photon energy the $2p$ ionization cross section is much larger than the cross sections for the ionization of the outer $3s$ and $3p$ shells. The line positions of the individual components of the $L_{23}M_{23}M_{23}$ Auger structure in the kinetic-energy region $270 < E_{kin} < 290$ eV [in Fig. 7(d); 80 eV $\leq E_B \leq$ 100 eV] and their relative intensities are almost identical to those found in the Auger spectra excited by electron impact [58]. This is interesting because Weber *et al.* [58] in order to account for the origin of the structures on the high-kinetic-energy side of the $L_{23}M_{23}M_{23}$ lines [$E_{kin} > 283$ eV, i.e., in Fig. 7(d) at $E_B < 87$ eV] discussed decay processes such as $2p^5 3d 4s^2 \rightarrow 2p^6 3s^2 3p^4 3d 4s^2 + \epsilon l$ or $2p^5 4s^2 4p \rightarrow 2p^6 3s^2 3p^4 4s^2 4p + \epsilon l$. The excitation of a $2p$ electron to an outer ns, np, or nd state is possible by impact of electrons with kinetic energies larger than the $2p$ ionization energy but forbidden for photons with $\hbar\omega = 370$ eV. The spectrum in Fig. 7(d) therefore clearly demonstrates that discrete one-electron excitations can be excluded as the main source of the intensity at the high-kinetic-energy side of the $L_{23}M_{23}M_{23}$ Auger spectrum of Ca.

The central part of Fig. 7 displays the electron spectra emitted upon the decay of the Ca* $2p^5(^2P_{3/2})3d4s^2$ [Fig. 7(b)] and Ca* $2p^5(^2P_{1/2})3d4s^2$ [Fig. 7(c)] resonances. These spectra have already been discussed in some detail elsewhere [19]. They show a drastic increase of the intensities of the main $3s$ and $3p$ lines due to an enhancement by the autoionization processes Ca* $2p^5 3d 4s^2 \rightarrow Ca^+$ $2p^6 3s^1 3p^6 4s^2 + \epsilon l$ and Ca^+ $2p^6 3s^2 3p^5 4s^2 + \epsilon' l'$. Table II shows that about 6% of the decay is predicted to go into the latter channel in the single-configuration approximation while the equivalent contribution to the $3s3p^6 4s^2$ channel is much weaker. This peak gets its contribution

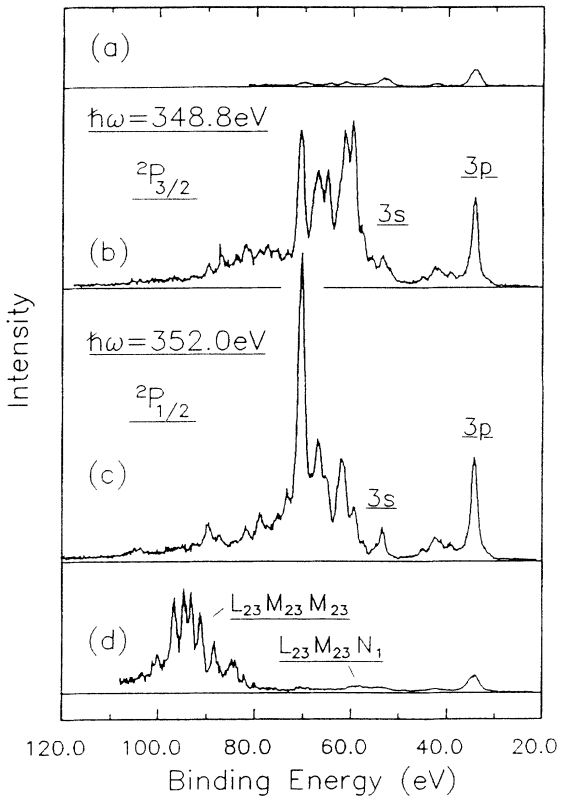

FIG. 7. Electron spectra of atomic Ca photoexcited at (a) $\hbar\omega = 344.2$ eV; (b) $\hbar\omega = 348.8$ eV, i.e., the Ca* $2p^5(^2P_{3/2})3s^2 3p^6 3d 4s^2\,{}^3D''$ resonance; (c) $\hbar\omega = 352.0$ eV, i.e., the Ca* $2p^5(^2P_{1/2})3s^2 3p^6 3d 4s^2\,{}^1P''$ resonance; and (d) $\hbar\omega = 370.0$ eV. The relative intensities are normalized via the $3p$ cross section shown in Fig. 12(a). ($\Delta\hbar\omega = 1.8$ eV; $U_{ret} = 200$ V.)

via CI as discussed before. The decay of the $2p \rightarrow 3d$ resonances also causes the large number of lines in the region 55 eV $< E_B <$ 110 eV, particularly the dominant line structure at 55 eV $< E_B <$ 75 eV, which has been assigned to decays into strongly mixed Ca^+ $3s^2 3p^4(4s^2 3d + 4p^2 3d + 3d^3)$ states [19]. The most striking feature is the dramatic change of the relative intensities between the final states when the excitation is changed from the Ca* $2p^5(^2P_{3/2})3d4s^2$ resonance to the Ca* $2p^5(^2P_{1/2})3d4s^2$ resonance. Although a glance at Fig. 3 shows fair agreement between the K and Ca spectra, our analysis suggests different causes in the two atoms for the change in the spectrum between the resonances.

The theoretical analysis of these autoionization processes is complicated because of the strong mixing which has to be taken into account for the initial 2p excited states and for the final ionic states. The calculations [19], which were carried out in *LS* coupling, therefore included a rather large number (427) of transitions. The following configurations were included in the initial state: $2p^5 3s^2 3p^6(3d4s^2 + 3d4p^2 + 3d4s^2 + 3d^3)$ and in the final state a continuum *p* electron with 287 eV energy coupled to the $2p^6 3s^2 3p^4(3d4s^2 + 3d4p^2 + 3d^3)$ and $2p^6 3s 3p^6(4s^2 + 4s3d + 4p^2 + 3d^2)$ configurations while no scaling were used as mentioned before. Table V summarizes the calculated energy positions and transition probabilities of the 22 strongest lines. The energies have been normalized to the observed $3s3p^6 4s^2$ binding energy. These lines comprise about 90% of the total intensity, i.e., of the sum of all 427 line intensities. There are three $J=1$ levels in the $2p^5 3d4s^2$ configuration with the $^3D_1$ and $^3P_1$ levels (in the *LS*-coupling scheme) close to each other and related to the $2p^5\,^2P_{3/2}$ parent term while $^1P_1$ corresponds to the $^2P_{1/2}$ parent term. The calculations show that the oscillator strength to the $^3P_1$ level is considerably smaller than the oscillator strength to $^3D_1$ so that in the calculations we assume that only the states $^3D_1$ (the lower resonance at $\hbar\omega = 348.8$ eV) and $^1P_1$ (the higher resonance at $\hbar\omega = 352.0$ eV) are populated. The configuration state labels given in Table V (column 2) represent the dominant basis state in the eigenvectors of the strongly mixed Ca^+ states. To illustrate the theoretical results, synthesized spectra for the decay of the two resonances are shown in Fig. 8(a) and compared with the observed spectra [Fig. 8(b)]. As an example of the complexity of the synthesized spectra, the details of the spectrum for the Ca* $2p^5(^2P_{1/2})3d4s^2(''^1P'')$ resonance is given in Fig. 8(c). The spectrum has been obtained by a convolution of 427 Voigt profiles with $\Gamma_L = 0.5$ eV (see Sec. V) and $\Gamma_G = 0.85$ eV. Energy positions and intensities of the lines are the calculated ones. The contributions corresponding to the decays to Ca^+ $3p^4 3d4s^2$, $3p^4 3d4p^2$, and $3p^4 3d^3$ final states are indicated separately. Transitions to the Ca^+ $3p^4 3d4s^2$ configuration dominate the spectrum in agreement with the calculated branching ratios (Table II). Positions and intensities of the 22 strongest lines given in Table V are shown as a histogram at the bottom of Fig. 8(c). Because of the complex nature of the experimental and the theoretical spectra a correlation between the two is difficult to establish and there is an obvious mismatch of the energies indicating that the theory without scaling as expected overestimates the splitting.

For this reason we have found it of interest to make calculations of the same type as for K (i.e., with scaling). In this calculation the same configurations as before were included in the initial state but in the final state only the $2p^6 3s^2 3p^4 3d4s^2$ and the $2p^6 3s 3p^6 4s^2$ configurations were included while for all the configurations the scaling factors found for the Ca IV $3s^2 3p^4(3d + 4s) + 3s3p^6$ configurations were applied. The results are shown in Fig. 8(d). The calculations show that the main features of the observed spectrum—the large intensity of the peak at 70 eV binding energy as well as the fact that this peak is more intense for the ^1P than for the ^3D resonance—are reproduced by the calculations. Also the width of the spectrum is quite well reproduced by the calculation, although slightly overestimated, but the main deficiency is that in the decay of the ^3D resonance the 70-eV peak is too strong. Also as in K, and for the same reason, the 3*s* peaks are too strong. We conclude that for Ca it is necessary to include interaction with additional configurations in order to obtain agreement with the observations although the simple scaling calculations reproduce some of the essential features.

TABLE V. Calculated relative binding energies of the Ca^+ final states and transition probabilities *A* for the decay of the Ca* $2p^5 3s^2 3p^6 3d4s^2\,^3D$ and ^1P resonances. The 22 strongest lines are listed. The lines are labeled by the largest eigenvector component of the strongly mixed Ca^+ final state. The labels in parentheses give the $3p^4$ parent term when appropriate. The energies are normalized to the observed energy for line 1. No scaling was used in the calculations as described in the text which is the reason that the calculated splittings are larger than the observed.

Line no.	Principal eigenvector component	E_b (eV)	A (10^{10} sec^{-1}) ^3D	^1P
1	$3s3p^6 4s^2\,^2S_{1/2}$	53.10[a]	624	1030
2	$3s^2 3p^4(^3P)3d4s^2\,^4D_{5/2}$	59.04	101	166
3	$(^3P)\,^4F_{5/2}$	61.43	538	290
4	$(^3P)\,^4F_{3/2}$	61.48	695	369
5	$(^3P)\,^4P_{1/2}$	62.44	624	296
6	$(^3P)\,^4P_{3/2}$	62.52	465	355
7	$(^1D)\,^2D_{3/2}$	62.84	102	170
8	$(^1D)\,^2F_{5/2}$	66.05	1330	741
9	$3s^2 3p^4(^3P)3d4p^2\,^4F_{3/2}$	66.53	0.4	142
10	$3s^2 3p^4(^1D)3d^3\,^2P_{3/2}$	68.66	128	104
11	$3s^2 3p^4(^1S)3d4s^2\,^2D_{3/2}$	68.69	374	206
12	$(^1S)\,^2D_{3/2}$	68.96	464	316
13	$3s^2 3p^4(^3P)3d4p^2\,^2P_{3/2}$	72.57	6	111
14	$(^1D)\,^2D_{3/2}$	73.08	243	774
15	$3s^2 3p^4(^3P)3d4s^2\,^2P_{3/2}$	73.12	122	511
16	$(^3P)\,^2P_{1/2}$	73.22	882	458
17	$3s^2 3p^4(^3P)3d^3\,^4P_{5/2}$	73.32	102	176
18	$(^3P)\,^2D_{3/2}$	73.63	114	129
19	$3s^2 3p^4(^1D)3d4p^2\,^2D_{5/2}$	74.24	63	139
20	$(^1D)\,^2D_{3/2}$	74.28	17	100
21	$3s^2 3p^4(^3P)3d4s^2\,^2D_{5/2}$	74.58	1060	1910
22	$(^3P)\,^3D_{3/2}$	74.86	907	1252

[a]Used for calibration.

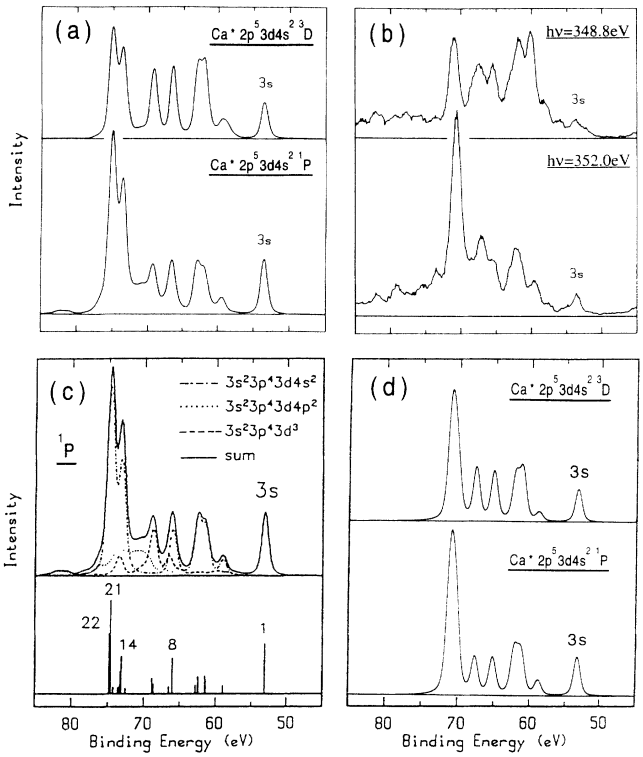

FIG. 8. Resonant Ca spectra for the $2p^5(^2P_{3/2},^2P_{1/2})3s^23p^63d4s^2$ resonances: (a) calculated spectra, (b) observed spectra, and (c) theoretical spectrum (top) constructed from the calculated decay rates of the excited Ca* $2p^53s^23p^63d4s^2\,^1P$ state without the use of scaling; see text. The contributions arising from the decay to different individual final states are indicated. The histogram (bottom) represents the calculated transition probabilities of the lines listed in Table V. (d) Calculated spectra including scaling; see text.

Additional information about the final states of the decay processes and about the primary Auger decay can be extracted from the low-kinetic-energy region of the electron spectrum. For the excitation energies $\hbar\omega=361$ and 370 eV, i.e., above the Ca^+ $2p^54s^2$ thresholds, the second-step Auger lines are presented in Fig. 9. The spectra are quite similar, except small additional lines in the upper spectrum ($\hbar\omega=370$ eV) at $E_{kin}>22$ eV and the broad structure at $E_{kin}\simeq 10$ eV, which is due to the direct Ca^+ $2p^5(^2P_{3/2})4s^2$ photoline. For calibration of the energy scale the two lines marked by a vertical arrow are used. They are assigned to the Auger decays of the $3p$ hole state, Ca^+ $3p^5(^2P_{3/2},^2P_{1/2})4s^2\rightarrow Ca^{2+}$ $3p^6+\epsilon l$ at $E_{kin}=13.33$ and 13.64 eV, respectively [52]. The other intense lines in the region 13 eV $<E_{kin}<$ 20 eV, which, relative to the $3p$ Auger lines gain some intensity at the higher photon energy, arise from the decay of the Ca^{2+} $3p^44s^2$ states populated in the $L_{23}M_{23}M_{23}$ Auger decay. Splitting and absolute energy positions suggest a transition Ca^{2+} $3p^4(^1S,^1D,^3P)4s^2\rightarrow Ca^{3+}$ $3p^5\,^2P_{3/2},^2P_{1/2}$. This assignment is corroborated by HF calculations (with the same scaling as before; 15% reduction of the direct interaction in the $3p^44s^2$ configuration), which determine relative energies for the Ca^{2+} $3p^44s^2$ multiplet components and the branching to the $^2P_{3/2}$ and $^2P_{1/2}$ levels of the Ca^{3+} $3p^5$ final state. In Table VI the experimental line positions and relative intensities are compared with the theoretical results. A shift of about -0.6 eV for the calculated energies of the $3p^44s^2$ configuration and -0.5 eV for the $3p^54s^2$ configuration results in quite good agreement for all transition energies. In Fig. 9 the vertical lines on top of the spectra represent the shifted theoretical energies for these transitions.

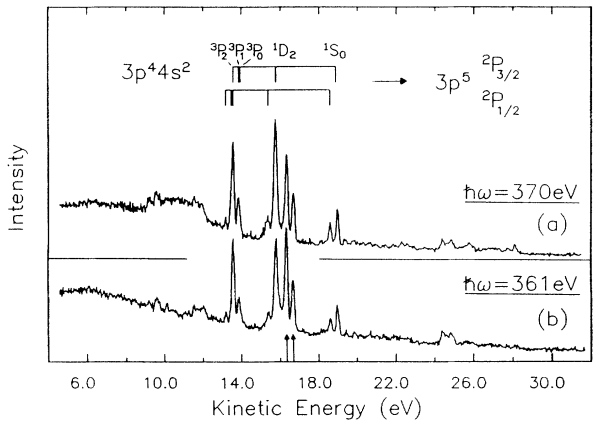

FIG. 9. Low-energy spectra of atomic Ca photoexcited at (a) $\hbar\omega=370$ eV and (b) $\hbar\omega=361$ eV. The vertical arrows (bottom) indicate the positions of the transitions Ca^+ $3p^5(^2P_{3/2},^2P_{1/2})4s^2\rightarrow Ca^{2+}$ $3p^6+\epsilon l$. The calculated Ca^{2+} $3p^44s^2\rightarrow Ca^{3+}$ $3p^5$ line positions are indicated at the top.

For a comparison of the branching ratios, the theoretical values given in Table VI were set equal to 100 for the sum over all transitions from each Ca^{2+} $3p^44s^2\,^{2S+1}L_J$ initial state. The same normalization was used for the experimental intensities except that the decay of the ^3P term, which is not completely resolved, was normalized to 300. Applying this normalization the trends in the observed branching ratios are well reproduced by the calculations. The theoretical branching ratios are nearly independent of whether scaling is used or not. Based on the experimental data the initial population of the Ca^{2+} $3p^4(^1S,^1D,^3P)4s^2$ levels was estimated to $^1S:^1D:^3P$

TABLE VI. Experimental and theoretical kinetic energies and relative intensities for the second-step decay Ca^{2+} $3p^4(^1S,^1D,^3P)4s^2 \rightarrow Ca^{3+}3p^5\,^2P_{3/2}$, $^2P_{1/2}$ following the normal $L_{23}M_{23}M_{23}$ Auger decay. The first-step Auger decay Ca^+ $3p^5 4s^2 \rightarrow Ca^{2+}$ $3p^6$ is included also. The theoretical values are obtained in the single-configuration HF approximation. The intensity normalization is described in the text.

Expt.		Theory		
E_{kin} (eV)	I_{rel}	E_{kin} (eV)	I_{rel}	Transition
13.19	30	13.76	13	$3p^4 4s^2\,^3P_2 \rightarrow 3p^5\,^2P_{1/2}$
		14.03	50	$3p^4 4s^2\,^3P_1 \rightarrow 3p^5\,^2P_{1/2}$
13.56	185	14.12	87	$3p^4 4s^2\,^3P_2 \rightarrow 3p^5\,^2P_{3/2}$
		14.13	60	$3p^4 4s^2\,^3P_0 \rightarrow 3p^5\,^2P_{1/2}$
13.87	85	14.39	50	$3p^4 4s^2\,^3P_1 \rightarrow 3p^5\,^2P_{3/2}$
		14.49	40	$3p^4 4s^2\,^3P_0 \rightarrow 3p^5\,^2P_{3/2}$
15.39	16	16.08	37	$3p^4 4s^2\,^1D_2 \rightarrow 3p^5\,^2P_{1/2}$
15.78	84	16.44	63	$3p^4 4s^2\,^1D_2 \rightarrow 3p^5\,^2P_{3/2}$
16.33	67	16.85	67	$3p^5 4s^2\,^2P_{3/2} \rightarrow 3p^6\,^1S_0$
16.69	33	17.20	33	$3p^5 4s^2\,^2P_{1/2} \rightarrow 3p^6\,^1S_0$
18.63	39	19.33	40	$3p^4 4s^2\,^1S_0 \rightarrow 3p^5\,^2P_{1/2}$
19.01	61	19.70	60	$3p^4 4s^2\,^1S_0 \rightarrow 3p^5\,^2P_{3/2}$

$=12{:}46{:}42$, fairly close to the experimental ratios [43] for the $L_2M_{23}M_{23}$ decay in Ar 15:48:37. The simplicity of this interpretation is remarkable given the complexity of the first step that has been interpreted as populating a large number of strongly interacting states which seems unnecessary for an understanding of the second step. It would clearly be interesting to study the spectrum as function of photon energy near to threshold.

The low-energy part of the electron spectra emitted following the decay of the Ca* $2p^5(^2P_{3/2},^2P_{1/2})3d4s^2$ resonances is much more complicated (Fig. 10). For orientation the Auger lines Ca^+ $3p^5(^2P_{3/2},^2P_{1/2})4s^2 \rightarrow Ca^{2+}$ $3p^6+\epsilon l$ are again marked by vertical arrows. Ca^+ $3p^5 3d4s \rightarrow Ca^{2+}$ $3p^6+\epsilon l$ transitions probably contribute to the neighboring line at 15.7 eV. Qualitatively the second-step spectra reflect some of the characteristic features, for example, the width, of the first-step spectra [see Figs. 7(b) and 7(c)]. Due to the numerous Ca^+ initial states, which can decay into several Ca^{2+} continua, it is very difficult to unravel the spectra. Only the broad peak at $E_{kin} \simeq 22$ eV is clearly related to the strong line located at $E_B \simeq 70$ eV in the autoionization spectra [Figs. 7(b) and 7(c)]. Therefore we ascribe this feature to the Ca^+ $3p^4(^3P)3d4s^2\,^2D$, $^2P \rightarrow Ca^{2+}3p^5 4s + \epsilon l$ transitions. This is supported by the extreme width of this line. A single configuration calculation for the lifetimes of the Ca^+ $3p^4 3d4s^2$ multiplet components results in a width of about 0.5–0.6 eV for the Ca^+ $3p^4(^3P)3d4s^2\,^2D$, ^2P terms and a width of less than 0.1 eV for all other states.

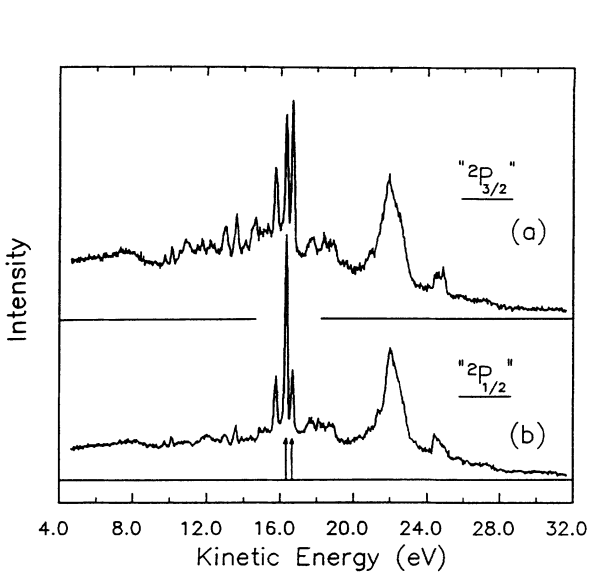

FIG. 10. Low-energy electron spectra of atomic Ca photoexcited at (a) $\hbar\omega = 348.8$ eV, i.e., the Ca* $2p^5(^2P_{3/2})3s^2 3p^6 3d4s^2\,''^3D''$; and (b) $\hbar\omega = 352.0$ eV, i.e., the Ca* $2p^5(^2P_{1/2})3s^2 3p^6 3d4s^2\,''^1P''$ resonance. The vertical arrows (bottom) indicate the positions of the transitions Ca^+ $3p^5(^2P_{3/2},^2P_{1/2})4s^2 \rightarrow Ca^{2+}$ $3p^6+\epsilon l$.

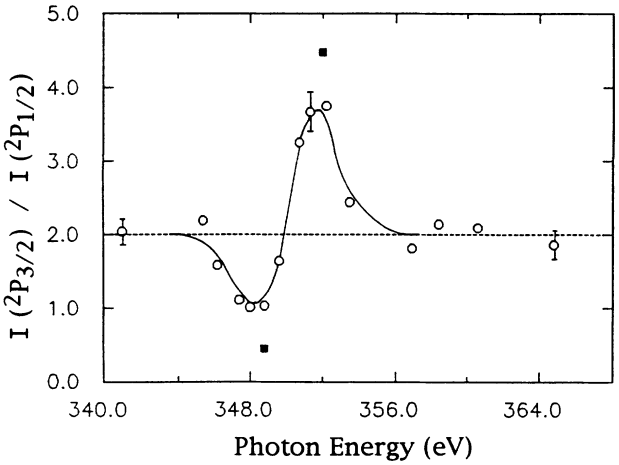

FIG. 11. Branching ratio $^2P_{3/2}$:$^2P_{1/2}$ for the decays Ca^+ $3p^5(^2P_{3/2},^2P_{1/2})4s^2 \rightarrow Ca^{2+}$ $3p^6+\epsilon l$ in the energy range of the $2p$ resonances; (○) experimental values and (■) theoretical values.

We note also the large change in the branching ratio for the decay Ca^+ $3p^5(^2P_{3/2})4s^2 \rightarrow Ca^{2+}3p^6+\epsilon l$ and Ca^+ $3p^5(^2P_{1/2})4s^2 \rightarrow Ca^{2+}$ $3p^6+\epsilon' l$. In the off-resonance spectrum (Fig. 9) the ratio is determined by the statistical weight of the initial state $^2P_{3/2}$:$^2P_{1/2} = 2{:}1$ whereas in the spectra emitted upon the decay of the Ca* $2p^5(^2P_{3/2},^2P_{1/2})3d4s^2$ resonances (Fig. 10) we find the ratios 1:1 and 3.7:1, respectively. The general behavior of the $^2P_{3/2}$:$^2P_{1/2}$ ratio in the photon energy region around the $2p \rightarrow 3d$ resonances is given in Fig. 11, which comprises the results of a set of different electron spectra. The calculations (given by the full squares) reproduce the experimental trends, but overestimate the deviations from the statistical ratio.

V. COMPARISON Ar-K-Ca

The relative partial cross sections σ_{3p} and σ_{3s} of atomic Ar, K, and Ca in the energy region of the $2p$ resonances and $2p$ thresholds are shown in Figs. 12 and 13. The curves for σ_{3p} (Fig. 12) have been obtained by recording constant-ionic-state (CIS) spectra, i.e., measur-

ing the intensity of the $3p$ photoelectron lines as a function of photon energy. The bandwidth of the monochromator decreased from $\Delta\hbar\omega = 1.0$ eV at $\hbar\omega \simeq 350$ eV (Ca) to about 0.6 eV at 250 eV (Ar). The energy positions of the $2p$ resonances and the $2p$ thresholds derived from the absorption spectra [5,7,10] are indicated. For atomic Ca the $3p$ cross section [Fig. 12(a)] is characterized by strong enhancements at the excitation energies $\hbar\omega = 348.8$ and 352.0 eV of the Ca* $2p^5(^2P_{3/2},^2P_{1/2})3d4s^2$ resonances. The interference between the resonantly driven Ca* $2p^5 3d4s^2 \rightarrow Ca^+$ $2p^6 3s^2 3p^5 4s^2 + \epsilon l$ autoionization channel and the direct Ca $3p^6 4s^2 \rightarrow Ca^+$ $3p^5 4s^2 + \epsilon l$ ionization manifests itself in the asymmetric profile of the lines. Except for the missing enhancement at the position of the $2p \rightarrow 4d$ excitations the $3p$ cross section resembles the absorption [10] and ion-yield [8,9] spectra. Since the oscillator strength for the $2p \rightarrow 4d$ excitation is much smaller than for $2p \rightarrow 3d$ and in addition the probability for the Ca* $2p^5 4s^2 4d \rightarrow Ca^+$ $2p^6 3s^2 3p^5 4s^2 + \epsilon l$ autoionization has been calculated to be three orders of magnitude smaller than the Ca* $2p^5 4s^2 4d \rightarrow Ca^+$ $2p^6 3s^2 3p^4 4s^2 4d$ Auger decay, the $3p$ cross section determined is consistent with the results of other methods. A striking feature of the $2p$ excitation spectra is the strong deviation of the Ca* $2p^5(^2P_{3/2})3d4s^2$:Ca* $2p^5(^2P_{1/2})3d4s^2$ intensity ratio from the statistical value 2:1. From the area of the resonances in the σ_{3p} cross section a ratio of 1:1.2 was determined [19] while Matsuo *et al.* [8] have found a ratio of 1:1.18 from the ion-yield spectrum. This finding can be explained [19] by describing the resonances in intermediate coupling. The collapse of the $3d$ wave function in the $2p^5 3d4s^2$ excited states gives rise to a $2p \leftrightarrow 3d$ interaction comparable to the $2p$ spin-orbit interaction. The characteristic features of the partial $3p$ cross section σ_{3p} are reproduced by calculations performed within the local-density random-phase approximation (LDRPA) [59]. The discrepancy in the width of the resonances is mainly due to the experimental broadening. The absolute values for the $3p$ cross section given on the right-hand side of the figure refer to the calculated cross section.

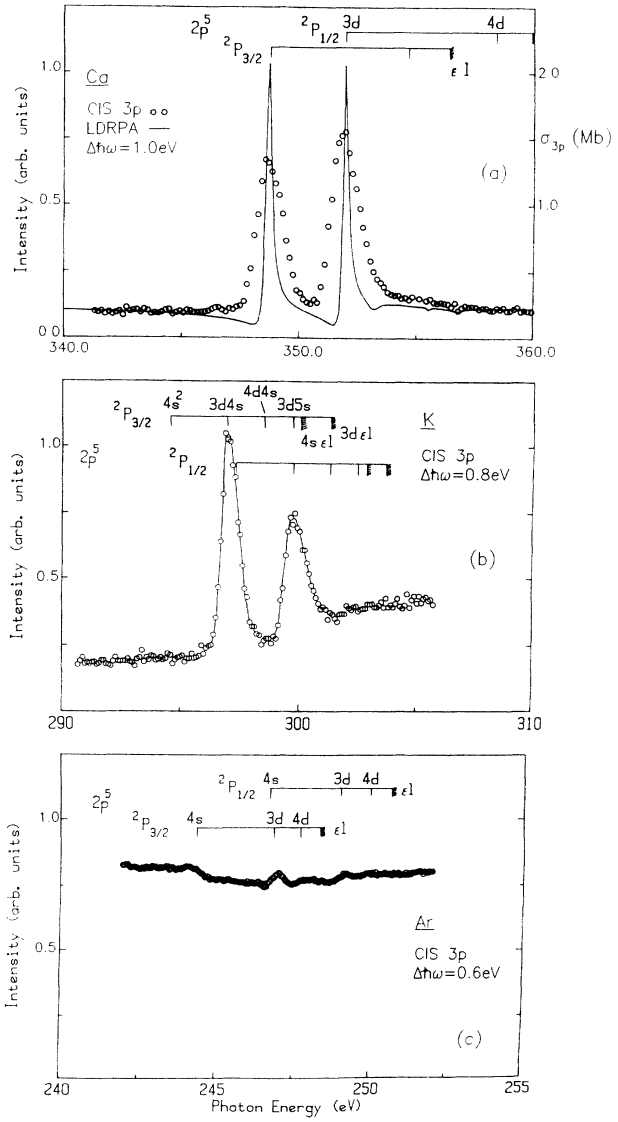

FIG. 12. Relative partial $3p$ cross sections of atomic Ar, K, and Ca represented by constant-ionic-state spectra of the photolines which leaves the ions in the states (a) Ca^+ $3p^5 4s^2 (E_b = 34.4$ eV), (b) K^+ $3p^5 4s, 3d (E_b = 24.7$ eV), and (c) Ar^+ $3p^5 (E_b = 15.8$ eV). The solid line is a LDRPA prediction [59] (see text), and the absolute values given on the right-hand side refer to this calculation.

The partial cross section σ_{3p} of atomic K [Fig. 12(b)] shows similar asymmetric resonances at the energies of the K $2p^6 4s \rightarrow K^*$ $2p^5(^2P_{3/2})3d4s$ and (the nominal) K* $2p^5(^2P_{1/2})3d4s$ excitations although the intensity ratio is close to the statistical value. However, the $^2P_{1/2}$ peak is apparently due to a number of final states, as discussed earlier, which means that it is difficult to use the intensity ratio to draw any conclusions for example about the degree of $3d$ collapse. We note that Matsuo *et al.* [8] reported that the ratios in the ion-yield spectra were similar in K and Ca. However, new high-resolution spectra [9] confirm the results in Fig. 12(b).

Finally, the CIS spectrum of atomic Ar [Fig. 12(c)] shows only very small resonant structures at the energy positions of the $2p \rightarrow 3d$ excitations. The $3p$ partial cross section is mainly determined by the direct ionization Ar $3s^2 3p^6 + \hbar\omega \rightarrow Ar^+$ $3p^5 + \epsilon l$. Table II shows that branchings for which $3d$ participates in the decay are very small, for the decay to $3s^2 3p^5$ only about 0.1%, which is in good agreement with the weak coupling between resonant and nonresonant decay in the CIS spectrum [Fig. 12(c)]. For K and Ca, the branching ratios are larger, 3.3% and 5.9%, respectively. This demonstrates the decreasing overlap between the wave function of the $2p$ hole and the excited $3d$ electron in the sequence Ca-K-Ar. For Ar the overlap between the $3d$ electron and the core is small and the $3d$ electron does not participate (except through shake effects) in the resonant Auger decay, although it influences the structure of the spectrum.

From the CIS spectra of Ca and K [Figs. 12(a) and 12(b)] it was possible to determine an upper limit for the natural lifetimes of the $2p$ excited states by taking into account the bandpass of the monochromator. For the Ca* $2p^5(^2P_{3/2})3d4s^2$ resonance we found a value

$\Gamma_R(2p \rightarrow 3d) < 0.5$ eV, which is corroborated by HF calculations [19]. Also for the K* $2p^5(^2P_{3/2})3d4s$ resonance we obtained a value $\Gamma_R(2p \rightarrow 3d) < 0.5$ eV. These values are markedly smaller than the linewidths determined by the absorption experiments [7,10].

The 3s cross sections of the three elements investigated are displayed in Fig. 13. In the case of Ca [Fig. 13(a)] and K [Fig. 13(b)] they have been determined from a set of electron spectra taken at different photon energies and normalized to the 3p cross sections. For Ar a CIS spectrum of the Ar^+ $3s^13p^6$ photoline is shown [Fig. 13(c)]. The intensities are given relative to the intensities for the 3p cross sections in Fig. 12 and the absolute values on the right-hand side of Fig. 13(a) refers to the calculated spectrum. The relative 3s cross section show the same characteristic trends as discussed for σ_{3p}, although the coupling to the resonant spectrum in this case is due primarily to CI, as discussed before, which is the reason that the coupling is strong in all three spectra. Taking into account the experimental broadening, the LDRPA calculations [59] provide a reasonable description of the Ca 3s cross section. The main differences are, first, that the calculation overestimates the 3s intensity outside the resonances. Second, the marked asymmetric line shape of the calculated spectrum is not reproduced by the experiment, but this may be due to the energy resolution of the photon beam.

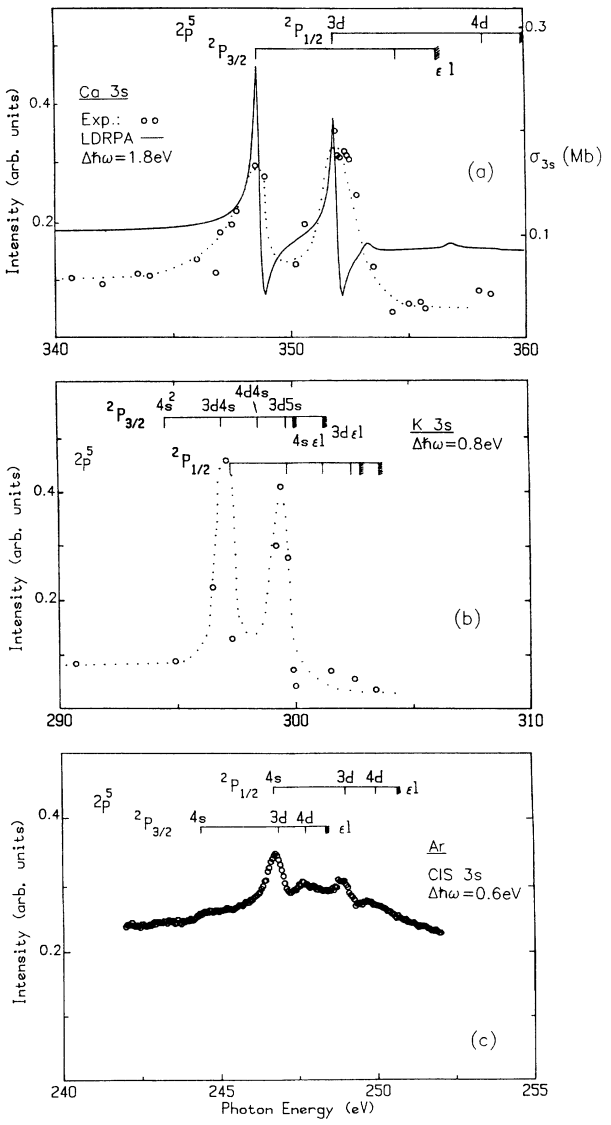

FIG. 13. Relative partial 3s cross sections of atomic Ar, K, and Ca. For (a) Ca and (b) K the cross sections are determined from a set of different photoelectron spectra and for (c) Ar a constant-ionic-state spectrum of the Ar^+ $3s^13p^6$ photoline ($E_b = 29.2$ eV) is shown. The solid line in (a) is a LDRPA prediction [59] (see text) and the absolute values refer to this calculation.

The increase in the localization of the 3d wave function along the series Ar, K, and Ca manifests itself in the increasing strength of the $2p \leftrightarrow 3d$ and the $3p \leftrightarrow 3d$ interaction. In the following we discuss the latter on the basis of the multiplet structure of the singly ionized states $3p^4nd4s^k$ ($k = 0$, 1, and 2 for Ar, K, and Ca, respectively). In Fig. 14 we show the relevant parts of the electron spectra emitted upon the decay of the Ar* $2p^5(^2P_{3/2})4d$ [Fig. 14(a)], Ar* $2p^5(^2P_{3/2})3d$ [Fig. 14(b)], K* $2p^5(^2P_{3/2})3d4s$ [Fig. 14(c)], and Ca* $2p^5(^2P_{3/2})3d4s^2$

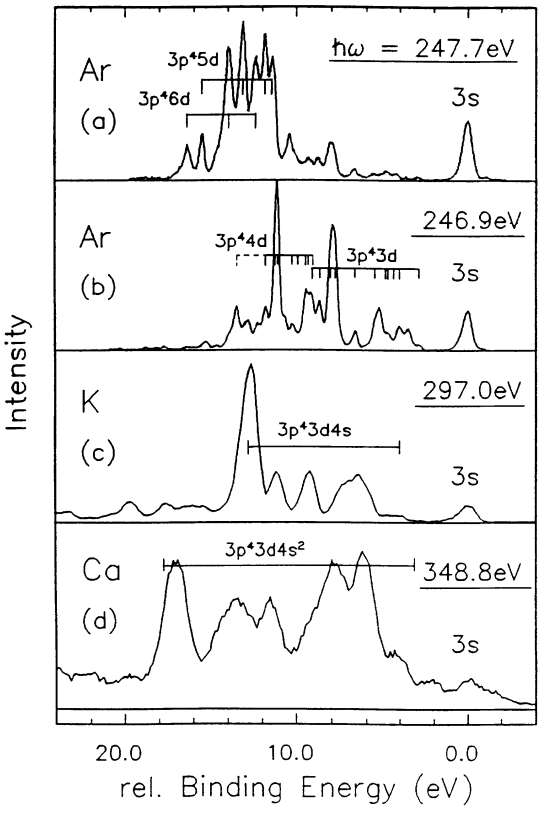

FIG. 14. Electron spectra photoecited at the excitation energies of (a) Ar* $2p^5(^2P_{3/2})3s^23p^64d$, (b) Ar* $2p^5(^2P_{3/2})3s^23p^63d$, (c) K* $2p^5(^2P_{3/2})3s^23p^63d4s$, and (d) Ca* $2p^5(^2P_{3/2})3s^23p^63d4s^2$. The spectra are given on a relative binding energy scale with the energy of the 3s photoline set to $E_{B,\mathrm{rel}} = 0$ eV. The estimated widths of the $3p^43d4s^k$ configurations with $k = 0$, 1, and 2 for Ar, K, and Ca, respectively, are indicated.

[Fig. 14(d)] resonances. The spectra are displayed on a relative binding energy scale, i.e., the spectra were shifted to normalize the $3s$ lines to the value $E_{B,\mathrm{rel}}=0$ eV. The two autoionization spectra of atomic Ar have already been discussed elsewhere [16]. Here we note the change in the strength of the $3p\leftrightarrow nd$ interaction in the Ar^+ $3p^4nd$ final states as a function of the principal quantum number n. For the $3p^45d$ and $3p^46d$ multiplets [Fig. 14(a)] the separation and the intensity distribution of the lines are mainly determined by the splitting and intensity distribution of the $3p^4\,{}^1S$, ${}^1D$, and ${}^3P$ parent terms. Only for the $3p^45d$ multiplet the small splitting of the ${}^3P$ parent term into two lines indicates a significant $p\leftrightarrow d$ interaction. On the other hand, we observe complicated line structures for the $3p^44d$ and $3p^43d$ final states [Fig. 14(b)]. Especially for the Ar^+ $3p^43d$ multiplet the collapse of the $3d$ wave function causes a similar strength for the $3p\leftrightarrow 3d$ and $3p\leftrightarrow 3p$ interaction. The role of the $3p^4$ parent terms in determining the structure of the spectrum is strongly reduced. Comparing the Ar^+ $3p^4nd$ multiplets with the corresponding structures in atomic Ca, i.e., with the Ca^+ $3p^43d4s^2$ final states, we first of all notice an increase of the total multiplet splitting, which is about 5 eV in the Ar spectra and about 14 eV for Ca. This tendency is due to the increasing nuclear charge Z going from Ar to Ca coupled with the effects of the $3d$ collapse.

The K^+ $3p^43d4s$ multiplet [Fig. 14(c)] should show an intermediate behavior. The splitting of the configuration is between the values for Ar and Ca, respectively. When the strong line at about 12 eV is identified as being close to the top of the configuration, the total width of the $3p^43d4s$ configuration in K II, which is indicated on the figure, is somewhat larger than the width of the $3p^43d$ configuration in Ar II, but considerably smaller than the width of $3p^43d4s^2$ in Ca II. If the existing analysis of $3p^43d$ in K III [29] is accepted, the width would be considerably larger than the width of $3p^43d$ in Ca IV, which contributed to our rejection of the high levels in the published analysis. Since the width of the $3p^43d4s^k$ configurations in a first approximation is determined by the splitting of the $3p^4$ configurations and the $3p\leftrightarrow 3p$ interaction does not change very much with the addition of an outer $4s$ electron, it can be understood that the width does not change very much before the $3p\leftrightarrow 3d$ exchange interaction becomes more important than the $3p\leftrightarrow 3p$ interaction. In fact the widths of the $3p^4$ configurations in Ar III, K IV, and Ca V are 4.1, 4.8, and 5.4 eV, respectively, and the isoionic variation can be expected to be even smaller. However, when considering the intensity distribution within the configuration, the importance of the parent mixing due to the $3p\leftrightarrow 3d$ exchange interaction becomes clear and here the similarity between K and Ca is greater than the similarity between K and Ar. In Ar, the main intensity is found in the region of the middle ${}^2D$ term while in K the intensity has moved to the region of the highest ${}^2D$ term. In Ca, the same is to some extent found in the calculation for the $2p^5({}^2P_{3/2})3d4s^2\,''{}^3D''$ resonance using scaling [Fig. 8(d)] while the rather low intensity observed in the high-energy region of this resonance appears to be due to additional configuration interaction. However, the enhancement of this peak is seen for the $2p^5({}^2P_{1/2})3d4s^2\,''{}^1P''$ resonance [Fig. 7(c)]. Thus the $2p^5({}^2P_{3/2})3d4s^2$ resonance in Ca is perhaps somewhat exceptional and not completely representative for the isoelectronic development of these spectra. It would be interesting to study the further development of this spectrum by considering $2p\rightarrow 3d$ excitations in ions such as Sc^+.

ACKNOWLEDGMENTS

This work was sponsored by the Stichting Nationale Computerfaciliteiten (National Computing Facilities Foundation, NCF) for the use of supercomputer facilities, with financial support from the Nederlandse Organisatie voor Wetenschappelijk Onderzoek (Netherlands Organization for Scientific Research, NWO). The continuous support of the HASYLAB staff is gratefully acknowledged. The authors are especially indebted to C. Kunz, S. Cramm, and I. Storjohann for being able to use the FLIPPER I station and for their help in operating it. This work was supported by the Bundesministerium für Forschung und Technologie der Bundesrepublik Deutschland.

[1] *Giant Resonances in Atoms, Molecules, and Solids,* edited by J. P. Connerade, J. M. Esteva, and R. C. Karnatak (Plenum, New York, 1987).

[2] B. Sonntag and P. Zimmermann, Rep. Prog. Phys. **55**, 911 (1992).

[3] M. Meyer, Th. Prescher, E. v. Raven, M. Richter, E. Schmidt, B. Sonntag, and H.-E. Wetzel, Z. Phys. D **2**, 347 (1986).

[4] M. Richter, M. Meyer, M. Pahler, T. Prescher, E. v. Raven, B. Sonntag, and H.-E. Wetzel, Phys. Rev. A **39**, 5666 (1989); **40**, 7007 (1989).

[5] M. Nakamura, M. Sasanuma, S. Sato, M. Watanabe, H. Yamashita, Y. Iguchi, A. Ejiri, S. Nakai, S. Yamaguchi, T. Sagawa, Y. Nakaii, and T. Oshio, Phys. Rev. Lett. **21**, 1303 (1968).

[6] T. Hayaishi, Y. Morioka, Y. Kageyama, M. Watanabe, I. H. Suzuki, A. Mikuni, G. Isoyama, S. Asaoka, and M. Nakamura, J. Phys. B **17**, 3511 (1984).

[7] M. W. D. Mansfield, Proc. R. Soc. London A **346**, 555 (1975).

[8] T. Matsuo, T. Hayaishi, Y. Itoh, T. Koizumi, T. Nagata, Y. Sato, E. Shigemasa, A. Yagishita, M. Yoshino, and Y. Itikawa, J. Phys. B **25**, 121 (1992).

[9] M. Kanno, G. Kutluk, T. Takaku, T. Nagata, E. Shigemasa, A. Yagishita, and F. Koike (unpublished).

[10] M. W. D. Mansfield, Proc. R. Soc. London A **348**, 143 (1976).

[11] U. Arp. F. Federmann, E. Källne, B. Sonntag, and S. L. Sorensen, J. Phys. B **25**, 3747 (1992).

[12] B. Sonntag, T. Nagata, Y. Sato, Y. Satow, A. Yagishita, and M. Yanagihara, J. Phys. B **17**, L55 (1984).

[13] B. K. Sarpal, C. Blancard, J. P. Connerade, J. M. Esteva,

J. Hormes, R. C. Karnatak, and U. Kuetgens, J. Phys. B **24**, 1593 (1991).
[14] H. Aksela, S. Aksela, H. Pulkkinen, G. M. Bancroft, and K. H. Tan, Phys. Rev. A **37**, 1798 (1988).
[15] T. A. Carlson, D. R. Mullins, C. E. Beall, B. W. Yates, J. W. Taylor, D. W. Lindle, and F. A. Grimm, Phys. Rev. A **39**, 1170 (1989).
[16] M. Meyer, E. v. Raven, B. Sonntag, and J. E. Hansen, Phys. Rev. A **43**, 177 (1991).
[17] H. Aksela, S. Aksela, A. Mäntykenttä, J. Tulkki, E. Shigemasa, A. Yagishita, and Y. Furusawa, Phys. Scr. **T41**, 113 (1992).
[18] J. A. de Gouw, J. van Eck, J. van der Weg, and H. G. M. Heideman, J. Phys. B **25**, 2007 (1992).
[19] M. Meyer, E. v. Raven, M. Richter, B. Sonntag, R. D. Cowan, and J. E. Hansen, Phys. Rev. A **39**, 4319 (1989).
[20] U. Becker, H. G. Kerkhoff, D. W. Lindle, P. H. Kobrin, T. A. Ferret, P. A. Heimann, C. M. Truesdale, and D. A. Shirley, Phys. Rev. A **34**, 2858 (1986).
[21] S. Süzer, B. Breuckmann, W. Menzel, C. E. Theodosiou, and W. Mehlhorn, J. Phys. B **13**, 2061 (1980).
[22] F. Senf, K. Behrens v. Rautenfeld, S. Cramm, C. Kunz, J. Lamp. V. Saile, J. Schmidt-May, and J. Voss, Nucl. Instrum. Methods A **246**, 314 (1986).
[23] H. Schröder, Ph.D. thesis, University of Hamburg, 1982.
[24] P. W. Palmberg, J. Electron Spectrosc. Relat. Phenom. **5**, 691 (1974); J. Vac. Sci. Technol. **12**, 379 (1975).
[25] P. A. Heimann, D. W. Lindle, T. A. Ferrett, S. H. Liu, L. J. Medhurst, M. N. Piancastelli, D. A. Shirley, U. Becker, H. G. Kerkhoff, B. Langer, D. Szostak, and R. Wehlitz, J. Phys. B **20**, 5005 (1987).
[26] R. D. Cowan, *The Theory of Atomic Structure and Spectra* (University of California Press, Berkeley, 1981).
[27] K. Rajnak and B. G. Wybourne, Phys. Rev. **132**, 280 (1963); **134**, A596 (1964).
[28] R. D. Cowan, J. Opt. Soc. Am. **58**, 924 (1968).
[29] J. Sugar and C. Corliss, J. Phys. Chem. Ref. Data **14**, Suppl. No. 2 (1985).
[30] R. Smitt, private communication to J. Sugar and C. Corliss, J. Chem. Phys. Ref. Data **8**, 865 (1979).
[31] H. Smid and J. E. Hansen, J. Phys. B **16**, 3339 (1983).
[32] L. Minnhagen, Ark. Fys. **25**, 203 (1963).
[33] R. D. Cowan and D. C. Griffin, J. Opt. Soc. Am. **66**, 1010 (1976).
[34] C. Froese Fischer, Comput. Phys. Commun. **64**, 369 (1991).
[35] D. C. Griffin, K. L. Andrew, and R. D. Cowan, Phys. Rev. **177**, 62 (1969).
[36] T. Hayaishi, E. Murakami, A. Yagishita, F. Koike, Y. Morioka, and J. E. Hansen, J. Phys. B **21**, 3203 (1988).
[37] G. C. King, M. Tronc, F. H. Read, and R. C. Bradford, J. Phys. B **10**, 2479 (1977).
[38] E. v. Raven, M. Meyer, M. Pahler, and B. Sonntag, J. Electron Spectrosc. Relat. Phenom. **52**, 677 (1990).
[39] S. B. Whitfield, C. D. Caldwell, and M. O. Krause, Phys. Rev. A **43**, 2338 (1991).
[40] S. B. Whitfield, J. Tulkki, and T. Åberg, Phys. Rev. A **44**, R6983 (1991).
[41] M. Meyer, E. v. Raven, M. Richter, B. Sonntag, and J. E. Hansen, J. Electron Spectrosc. Relat. Phenom. **51**, 407 (1990).
[42] M. Meyer, E. v. Raven, B. Sonntag, and J. E. Hansen, in *Proceedings of the Second European Conference on Progress in X-Ray Synchrotron Research,* edited by A. Balerna, E. Bernieri, and S. Mobilio (SIF, Bologna, 1990), Vol. 25, p. 153.
[43] J. Tulkki, T. Åberg, A. Mäntykenttä, and H. Aksela, Phys. Rev. A **46**, 1357 (1992).
[44] B. Brueckmann, Ph.D. thesis, University of Freiburg (1978).
[45] S. Aksela, M. Kellokumpu, H. Aksela, and J. Väyrynen, Phys. Rev. A **23**, 2374 (1981).
[46] A. Russek and W. Mehlhorn, J. Phys. B **19**, 911 (1986).
[47] M. Borst and V. Schmidt, Phys. Rev. A **33**, 4456 (1986).
[48] V. Schmidt, Z. Phys. D **2**, 275 (1986).
[49] M. W. D. Mansfield and G. H. Newsom, Proc. R. Soc. London Ser. A **357**, 77 (1977).
[50] M. W. D. Mansfield and T. W. Ottley, Proc. R. Soc. London Ser. A **365**, 413 (1979).
[51] Y. Sato, T. Hayaishi, Y. Itikawa, Y. Itoh, J. Murakami, T. Nagata, T. Sasaki, B. Sonntag, A. Yagishita, and M. Yoshino, J. Phys. B **18**, 225 (1985).
[52] J. M. Bizau, P. Gérard, F. J. Wuilleumier, and G. Wendin, Phys. Rev. A **36**, 1220 (1987).
[53] P. C. Deshmukh and W. R. Johnson, Phys. Rev. A **27**, 326 (1983).
[54] Z. Altun, S. L. Carter, and H. P. Kelly, Phys. Rev. A **27**, 1943 (1983).
[55] J. E. Hansen, Phys. Scr. **21**, 510 (1980).
[56] R. D. Cowan, J. E. Hansen, and H. Smid, Phys. Rev. A **31**, 2750 (1985).
[57] J. E. Hansen and P. Scott, Phys. Rev. A **33**, 3133 (1986).
[58] W. Weber, B. Breuckmann, R. Huster, W. Menzel, W. Mehlhorn, M. H. Chen, and K. G. Dyall, J. Electron Spectrosc. Relat. Phenom. **47**, 105 (1988).
[59] G. Wendin (private communication).